

# Traces of urban forest in temperature and CO<sub>2</sub> signals in monsoon East Asia

Keunmin Lee<sup>1</sup>, Je-Woo Hong<sup>2</sup>, Jeongwon Kim<sup>1</sup>, Sungsoo Jo<sup>1</sup>, and Jinkyu Hong<sup>1</sup>

<sup>1</sup>Department of Atmospheric Sciences, Yonsei University, Seoul, 03722, Korea (Republic of)

<sup>2</sup>Korea Environment Institute, Sejong, 30147, Korea (Republic of)

*Correspondence to:* Jinkyu Hong (jhong@yonsei.ac.kr)

**Abstract.** Cities represent a key space for a sustainable society in a changing environment, and our society is steadily embracing urban green space for its role in mitigating heatwaves and anthropogenic CO<sub>2</sub> emissions. This study reports two years of surface fluxes of energy and CO<sub>2</sub> in an artificially constructed urban forest measured by the eddy covariance method to examine the impact of urban forests on air temperature and net CO<sub>2</sub> exchange. The urban forest site shows typical seasonal patterns of forest canopies with the seasonal march of the East Asian summer monsoon. This study shows that the urban forest reduces both the warming trend and urban heat island intensity compared to the adjacent high-rise urban areas and that photosynthetic carbon uptake is large despite relatively small tree density and leaf area index. During the significant drought period in the second year, gross primary production and evapotranspiration decreased, but their reduction was not as significant as those in natural forest canopies. We speculate that forest management practices, such as artificial irrigation and fertilization, enhance vegetation activity. Further analysis reveals that ecosystem respiration in urban forests is more pronounced than for typical natural forests in a similar climate zone. This can be attributed to the substantial amount of soil organic carbon due to intensive historical soil use and soil transplantation during forest construction, as well as relatively warmer temperatures in urban heat domes. Our findings suggest the need for caution in soil management when aiming to reduce CO<sub>2</sub> emissions in urban areas.

## 1 Introduction

Cities make up only 2% of the Earth's land surface but hold more than 55% of the world's population. It is expected that the urban population will reach 68% by 2050 (UN, 2019). With the unprecedented rapid urbanization in the last century, human civilization heavily depends on urban structures and functions. Current concern is regarding the disastrous impacts of climatic events (e.g., heatwaves, flooding, and drought) and environmental changes (e.g., air pollution and land degradation) on our socioeconomic system in a changing climate (McCarthy et al., 2010; Rahmstorf and Coumou, 2011). Accordingly, it remains an urgent issue to implement integrated policies for climate change mitigation and adaption toward sustainable cities against global warming and related natural disasters.

Urban green infrastructures, such as urban forests, have been recognized as a key solution toward alleviating climatic and environmental disasters (e.g., Chiesura, 2004; Haaland and van den Bosch, 2015; Oke et al., 2017;

34 Kroeger et al., 2019). Green spaces in cities are exposed to wide ranges of environmental and climatic conditions  
35 across geographical locations. Especially when green spaces replace gray infrastructures during urban  
36 redevelopment, it remains unclear whether their benefits emerge in real conditions and thereby overcome their  
37 maintenance cost and other harmful effects (e.g., allergy and ozone increase). To leverage their full potential  
38 benefits, it is necessary to assess the biophysical effects of urban forests based on direct long-term monitoring in  
39 urban areas.

40 Urban forests are a key part of green infrastructures in a city, and two of their benefits, which have been addressed  
41 in previous studies, are thermal mitigation and carbon uptake (Roy et al., 2012; Oke et al., 2017). Firstly, urban  
42 forests mitigate direct sunlight and diminish the incoming radiant energy on the land surface, thereby reducing  
43 surface temperature. Additionally, urban forests supply water to the atmosphere through transpiration and retain  
44 water for longer than the impervious surfaces of urban structures. These processes contribute to reducing air  
45 temperature by partitioning more available energy to latent heat flux ( $Q_E$ ) than sensible heat flux ( $Q_H$ ), thus  
46 creating favorable conditions for mitigating heatwaves and related health problems (e.g., Oke, 1982; Hong et al.,  
47 2019a). Eventually, this cooling effect reduces the electrical energy load by air conditioning as well as greenhouse  
48 gas emissions. Previous studies have reported cooling effects of urban forests from street trees to parks scales  
49 (Oke et al., 1989; Bowler et al., 2010; Norton et al., 2015; Shashua-Bar and Hoffman, 2000). Such cooling effects  
50 depend not only on tree species and structures (Feyisa et al., 2014) but also on the size and vegetation density of  
51 urban green areas (Yu and Hien, 2006; Chang et al., 2007; Hamada and Ohta, 2010; Feyisa et al., 2014). However,  
52 despite the strong temperature-controlling factors of evapotranspiration (ET) and sensible heat fluxes over urban  
53 forest canopies, only a few studies have reported on surface energy balance (SEB) in urban forests in relation to  
54 thermal mitigation based on direct measurements (e.g., Oke et al., 1989; Spronken-Smith et al., 2000; Coutts et  
55 al., 2007a; Ballinas and Barradas, 2015; Hong and Hong, 2016;). Moreover, it is noticeable that forest cooling  
56 intensity depends on geography and forests can even produce a warming trend as a result of their low albedo  
57 (Bonan, 2008; Wang et al., 2018). The lack of direct urban forest measurements hinders proper assessment of  
58 their influences on the climate and environment.

59 Furthermore, urban forests mitigate anthropogenic carbon emissions by photosynthetic CO<sub>2</sub> uptake. Traditionally,  
60 carbon uptake by urban forests has been estimated by empirical relationships (e.g., biomass allometric equation)  
61 or short-term inventory of biomass data and vegetation growth rates, which have limitations of spatiotemporal  
62 coverage (Rowntree and Nowak, 1991; Nowak, 1993; Nowak et al., 2008; Weissert et al., 2014). Currently, the  
63 eddy covariance (EC) method is being applied in various ecosystems from grasslands and natural forests to urban  
64 areas because it provides continuous net CO<sub>2</sub> flux measurements at the neighborhood scale every half hour  
65 (Christen 2014). From this perspective, the EC method is useful for studying the net CO<sub>2</sub> exchange ( $F_C$ ) from  
66 diurnal to interannual variations, with its simultaneous measurement of surface energy fluxes. Recently, direct  $F_C$   
67 measurements have been performed using the EC method in urban green spaces to examine turbulent exchanges  
68 of energy and carbon (Coutts et al., 2007a, 2007b; Awal et al., 2010; Kordowski and Kuttler, 2010; Bergeron and  
69 Strachan, 2011; Crawford et al., 2011; Peters and McFadden, 2012; Velasco et al., 2013; Ward et al., 2013;  
70 Ueyama and Ando, 2016; Hong et al., 2019b). However, the EC method provides only the net effects of CO<sub>2</sub>

71 exchange from various carbon sources and sinks, which limits the physical interpretation and assessment of the  
72 benefits and costs of urban forests. It is challenging to partition  $F_C$  into individual sources and sinks in urban areas  
73 because of the complex contributions from biogenic (e.g., vegetation photosynthesis, respiration of vegetation,  
74 soil, and humans) and extra anthropogenic (e.g., fossil fuel combustion by transportation or in households and  
75 commercial buildings) processes (Pataki et al., 2003).

76 With this background, the objectives of this study include: 1) reporting temporal changes in air temperature after  
77 the artificial construction of an urban forest park in the Seoul metropolitan area with a hot and humid summer and  
78 cold and dry winter seasons and 2) quantifying the carbon uptake of urban forests based on partitioning of  $F_C$  data  
79 measured by the eddy covariance method and meteorological data (Lee et al., 2021). Here, we highlight the biotic  
80 and abiotic factors controlling the carbon cycle in urban forests and the impact of urban forests on the thermal  
81 environment after forest park construction.

## 82 **2 Materials and Methods**

### 83 **2.1 Urban surface energy and CO<sub>2</sub> balances**

84 The SEB is expressed as:

$$85 \quad Q^* + Q_F = Q_H + Q_E + \Delta Q_S + \Delta Q_A \quad (1)$$

86 where  $Q^*$  is the net all-wave radiation of the sum of outgoing and incoming short- and long-wave radiative fluxes,  
87  $Q_F$  is the anthropogenic heat flux,  $Q_H$  is the turbulent sensible heat flux,  $Q_E$  is the latent heat flux,  $\Delta Q_S$  is the net  
88 storage heat flux, and  $\Delta Q_A$  is the net heat advection (Definitions of variables in Appendix A).

89 The surface CO<sub>2</sub> budget in an urban forest is formulated as follows:

$$90 \quad F_C = E_R + E_B + RE - GPP \equiv E_R + E_B + NBE \quad (2)$$

91 where  $F_C$  is the net CO<sub>2</sub> exchange at the city-atmosphere interface,  $E_R$  and  $E_B$  are the anthropogenic CO<sub>2</sub> emissions  
92 from fossil fuel combustion by vehicles and heating in a building, respectively.  $GPP$  and  $RE$  are biotic  
93 contributions to  $F_C$ ;  $GPP$  is the gross primary production by photosynthetic CO<sub>2</sub> uptake, and  $RE$  is the ecosystem  
94 respiration from soil and vegetation. Urban ecosystem respiration considers not only the autotrophic and  
95 heterotrophic respirations of vegetation and soil but also human respiration (Moriwaki and Kanda, 2004; Velasco  
96 and Roth, 2010; Ward et al., 2013, 2015; Hong et al., 2020). Human respiration by park visitor is negligible with  
97  $0.4 \mu\text{mol m}^2 \text{s}^{-1}$  at most .

98 Additionally,  $NBE$  is the net biome CO<sub>2</sub> exchange and is typically defined as the net ecosystem exchange by  $RE$   
99  $- GPP$  for natural vegetation. Put differently,  $NBE$  refers to carbon losses in heterotrophic respiration minus the  
100 net primary production on natural vegetative surfaces; thus, negative  $NBE$  indicates the net carbon uptake by the  
101 natural ecosystem (Kirschbaum et al., 2001; Randerson et al., 2002). Unlike natural ecosystems, the  $F_C$  between  
102 an urban forest and atmosphere is a complex mixture of biogenic (i.e.,  $GPP$  and  $RE$ ) and anthropogenic (i.e.,  $E_R$   
103 and  $E_B$ ) processes across various spatial and temporal scales. In urban environments, anthropogenic emissions

104 depend on the local characteristics (e.g., transport options, fuel types, heating demand, climate, population density,  
105 levels of industrial activity, and existing carbon intensity of electricity supply) of the city (Feigenwinter et al.,  
106 2012; Kennedy et al., 2014; Lietzke et al., 2015; Stagakis et al., 2019).

107

## 108 **2.2 Site description**

### 109 **2.2.1 Climate conditions**

110 Climatic condition shows a distinct seasonal variation with the seasonal march of the East Asian summer monsoon  
111 (Fig. 1). The mean climatological values (1981-2010) of the screen-level air temperature ( $T_{air}$ ) and precipitation  
112 were 12.5°C and 1450 mm year<sup>-1</sup>, respectively. During the study period (June 2013–May 2015), the observed  $T_{air}$   
113 was higher than the climatological mean. Higher temperatures lasted longer in the summer of 2013 with the  
114 stagnation of the migratory anticyclones (June) and North Pacific anticyclone (July–August). There were strong  
115 heatwaves in the spring seasons of 2014 and 2015 (Hong et al., 2019a). Wind direction also shows seasonal  
116 variation with the monsoon system. Main wind comes from vegetative surface in the park, but other land cover  
117 types are included differently with seasons. Prevailing wind is southwesterly in spring and summer and changes  
118 to northeasterly in autumn and northwesterly in winter (Fig. 2). Accordingly, road fraction in flux footprint is  
119 larger in spring and summer and building emission is included only winter season with northeasterly wind (Fig.  
120 3f and 2).

121 Notably, seasonal precipitation shows a contrasting pattern between two consecutive years (Fig. 1d). In the first  
122 year (June 2013–May 2014), annual precipitation was 1256 mm, which corresponded to approximately 90% of  
123 the climatological mean. In addition, approximately 50% of the annual rainfall was concentrated in the summer  
124 with an estimated 650 mm occurring only in July 2013; however, in the second year the annual rainfall was 932  
125 mm (i.e., 67% of the climatological mean) (i.e., the smallest annual precipitation in the past 20 years). The monthly  
126 precipitation values in the July and August of 2014 were 198 and 169 mm, respectively, which represented only  
127 approximately 35% of the climate mean. Accordingly, the vapor pressure deficit ( $VPD$ ) and downward shortwave  
128 radiation ( $K_d$ ) in July 2013 were relatively smaller than those in July 2014 (Fig. 2b and 2c).

### 129 **2.2.2 Seoul Forest Park**

130 Micrometeorological measurements were taken at the Seoul Forest Park (SFP) in the Seoul metropolitan area,  
131 Korea (37.5446°N, 127.0379°E). SFP is the third largest park in Seoul with an area of 1.16 km<sup>2</sup> (Fig. 3a). This  
132 area had been used as a horse racetrack and a golf course inside the track since 1950 and was surrounded by  
133 cement factories to the west (Fig. 3b). The local government initially planned this area as a commercial district  
134 with a high-rise multi-purpose building complex but changed its plan to redevelop the area as a green space in  
135 late 1990s. The construction of the SFP began in December 2003, and it was opened to the public in June 2005  
136 (Fig. 3c).

137 The mean tree height ( $h_c$ ) is approximately 7.5 m and ranges between 5.8–9.5 m. Analysis and estimation of  
138 roughness elements and integral turbulence characteristics are reported in Kent et al. (2018) and here we explain

139 the key information. 1-m horizontal resolution digital terrain and digital surface model data are analyzed for  
140 roughness parameters and tree heights. The mean roughness length ( $z_0$ ) and zero-plane displacement height ( $z_d$ )  
141 range between 0.3–0.6 and 4.1–8.2 m with wind directions, respectively.  $z_0$  and  $z_d$  have seasonal and directional  
142 variations depending on the variability of the leaves on the vegetation (Lee, 2015; Kent et al., 2018).  $z_0$  and  $z_d$   
143 change from approximately 0.6 and 5.0 m during leaf-on period (June–August) to 1.2 and 3.0 m during the leaf-  
144 off periods (December–February).

145 Approximately 80% of the footprint area of the SFP tower is within 250 m (Fig. 3e) and the dominant land cover  
146 within this range is a deciduous forest with irrigated grass lawns (*Zoysia*), oak (*Quercus acutissima*), ginkgo  
147 (*Ginkgo biloba*), and ash trees (*Fraxinus rhynchophylla*), which correspond to the Local Climate Zone (LCZ) ‘A’,  
148 dense trees (Stewart and Oke, 2012). The maximum leaf area index (LAI) of  $300 \times 300 \text{ m}^2$  around the SFP tower  
149 is approximately 1.6 (Copernicus Service information, 2020). On the east side ( $0\text{--}120^\circ$ ), there are trees  
150 (approximately  $230 \text{ stems ha}^{-1}$ ) with a small artificial lake and grasslands beyond it. Trees mainly occupy the  
151 south and west sectors of a tower ( $120\text{--}330^\circ$ ) within a 100-m radius area (approximately  $540 \text{ stems ha}^{-1}$ ) and  
152 traffic roads lie outside of the park (Fig. 3f).

153 The measurement system was installed on the rooftop of the SFP facility building (Fig. 3d). A three-dimensional  
154 sonic anemometer (CSAT3A, Campbell Scientific, USA) and enclosed infrared gas analyzer (EC155, Campbell  
155 Scientific, USA) were mounted 12.2 m above the ground level (2.8 m above the roof of an 8.4 m high building)  
156 in June 2013 for 2 years (Fig. 3d). The eddy covariance data were recorded using the data logger (CR3000,  
157 Campbell Scientific, USA) with a 10-Hz sampling rate and a 30-min averaging time. The gas analyzer was  
158 calibrated with standard  $\text{CO}_2$  gas every three months. The measurement height ( $z_m$ ) satisfied the tower height  
159 requirement over forested or more structurally complex ecosystems in most of wind directions (i.e.,  $z_m \cong z_d + 4(h_c$   
160  $- z_d)$ ) and turbulent flow is in the skimming flow region (Grimmond and Oke, 1999; Munger et al., 2012; Kent et  
161 al., 2018). Two radiometers (NR Lite2 and CMP3, Kipp&Zonen, Netherlands) were used to measure the radiative  
162 fluxes. An auxiliary measurement included a humidity and temperature probe (HMP155A, Vaisala, Finland) and  
163 EVI (Enhanced Vegetation Index) by in situ LED sensors.

164 The roads consist of eight and ten lanes carrying heavy traffic throughout the day ( $\sim 100,000 \text{ vehicles day}^{-1}$ ) to the  
165 south and west of the tower (Fig. 3c). Hourly traffic volume, which is used for surface flux partitioning, is  
166 evaluated on the road adjacent to the SFP tower every year by the Seoul Metropolitan Government  
167 (<https://topis.seoul.go.kr>). Across the road on the western side of the tower, a cement factory still exists, although  
168 its size is smaller than it used to be in the past (Fig. 3b and 3c).

### 169 **2.2.3 Observations in the Seoul Metropolitan Area**

170 Meteorological data from six stations (one eddy covariance station, one aerodrome meteorological observation  
171 station, and four automatic weather stations) in the Seoul Metropolitan Area are analyzed to examine the heat  
172 mitigation and  $\text{CO}_2$  reduction effects of urban vegetation in the SFP (Table 1 and Fig. 3a). The Eunpyeong eddy  
173 covariance site (EP,  $37.6350^\circ\text{N}$ ,  $126.9287^\circ\text{E}$ ) is for surface flux observations in the northwest of Seoul, where

174 there was a recent urban redevelopment to high-rise and high-population residential areas from low-rise areas  
175 (Hong and Hong, 2016; Hong et al., 2019b). Flux observations at the site have been conducted since 2012, and  
176 they show the surface energy fluxes and turbulence characteristics of a typical urban residential area. Because the  
177 area around the SFP was originally planned to be redeveloped to high-rise high-population residential buildings,  
178 EP is selected for comparative analysis as an antipodal place for the SFP region because the sites are close to each  
179 other and so have the similar synoptic conditions.

180 The Gimpo Airport weather station (GP, 37.5722°N, 126.7751°E) is located on the western boundary of Seoul,  
181 and it is surrounded by grasslands and croplands, which corresponds to LCZ 'D'. As the dominant wind comes  
182 from the west, the GP site is generally affected by the same synoptic weather conditions as Seoul. The GP station  
183 represents the rural environment of the Seoul Metropolitan Area because urban development is restricted around  
184 the airport. In this study, we select the GP site as a reference point and calculate the urban heat island intensity  
185 (UHI<sub>i</sub>) as the synchronous difference in  $T_{air}$  between the urban and rural areas accordingly (Stewart, 2011).

186 The Seongdong weather station (SD, 37.5472°N, 127.0389°E), the closest station to the SFP, is located  
187 approximately 300 m north of the SFP tower (Fig. 3c). Since the station began observations in August 2000, the  
188 meteorological data at SD are useful for analyzing temperature changes before and after the construction of the  
189 SFP. Accordingly, it is used to analyze local climatic changes caused by the SFP. Moreover, SD provides auxiliary  
190 weather variables (e.g., precipitation) that are not observed in SFP station and reference data for the gap filling.

191 The Gangnam, Seocho, and Songpa weather stations (hereafter denoted as CBD) are located in Seoul's central  
192 business district, which corresponds to LCZ 1 or 2. These sites are also close to the SFP (~ 5 km); thus,  
193 temperatures in these regions can be assumed to be exposed to the same synoptic condition. The annual mean  
194 maximum UHI<sub>i</sub> of CBD ranges from 3.7 to 5 °C and is similar to that of the SD. These regions show greater UHI<sub>i</sub>  
195 than other parts of Seoul because of dense skyscrapers (Hong et al., 2013; Hong et al., 2019a). The average  
196 temperature of these three automatic weather stations is used to evaluate the temperature and UHI<sub>i</sub> reduction  
197 effects of the SFP construction. All meteorological data from the automatic weather station and aerodrome  
198 meteorological observation station are observed every minute, and they are averaged for 1 h for UHI<sub>i</sub> analysis.  
199 All the meteorological data are processed for quality control on the National Climate Data Portal of the Korea  
200 Meteorological Administration (<http://data.kma.go.kr>).

### 201 **2.3 Data processing procedures**

202 Turbulent fluxes are computed using EddyPro (6.2.0 version, LI-COR), with the applications of the double  
203 rotation, time lag compensation using covariance maximization, quality test, and spectral corrections (Hong et al.,  
204 2020 and references therein). We apply the following post processes for quality control: 1) plausible value check,  
205 2) spike removal, and 3) discarding the negative  $F_c$  flux during the nighttime (i.e., no photosynthesis at night)  
206 (Hong et al., 2020). The total study period from installation (31 May, 2013) to termination (03 June, 2015) is  
207 approximately 2 years (35,174 potential 30-min data), and in December 2013, there was a gap for approximately

208 4 weeks due to the power system failure. The total available data are approximately 90.1%, 88.3%, and 85.4% (n  
209 = 31709, 31064, 30028) for  $Q_H$ ,  $Q_E$ , and  $F_C$ , respectively.

210 The flux partitioning and gap filling methods are well documented in previous studies of Lee et al. (2021) and  
211 Hong et al. (2019b) and here we describe the core of the methods. Missing values in turbulent exchange of energy  
212 and  $\text{CO}_2$  are filled with an artificial neural network (ANN) of a backpropagation algorithm. The ANN uses the  
213 cosine transformed time-of-the-day and day-of-the-year, air temperature, relative humidity, wind speed and  
214 direction, atmospheric pressure, precipitation, downward shortwave radiation, cloud cover, soil temperature, and  
215 EVI.

216 Flux partitioning into photosynthesis and ecosystem respiration from the EC measured  $F_C$  requires additional  
217 information and data processing (e.g., Stoy et al., 2006). Stochastic  $F_C$  partitioning methods were recently applied  
218 by reprocessing EC observation data with auxiliary data and provided useful knowledge on carbon cycle (Hiller  
219 et al., 2011; Crawford and Christen, 2015; Menzer and McFadden, 2017; Stagakis et al., 2019). Here we partition  
220 the measured  $F_C$  into four contributing components (i.e.,  $RE$ ,  $GPP$ ,  $E_R$ , and  $E_B$  in Eq. 2) to investigate their biotic  
221 and abiotic controlling factors in an artificially constructed park. Menzer and McFadden (2017) estimates  
222 anthropogenic emissions with traffic volume and air temperature in winter with wind directions when  
223 anthropogenic emission is dominant in net  $\text{CO}_2$  fluxes. This study extends the statistical partitioning method by  
224 Menzer and McFadden (2017). Similar to Menzer and McFadden (2017), our partitioning method chooses  
225 temporal subsets so that some components in Eqn. (2) are insignificant with footprint weighted road fraction so  
226 that the statistical partitioning is applicable even when  $E_R$  is not negligible. In this way,  $RE$  is estimated as a  
227 function of temperature first and  $GPP$  is finally estimated after modelling  $E_R$  and  $E_B$  based on the traffic volume  
228 and high-resolution footprint weighted road fraction (see Fig. 1a and Table 1 in Lee et al. (2021)). Our estimations  
229 on anthropogenic emission from vehicle and building show good correlation with inventory data such as visitor  
230 counts, traffic volume, and natural gas consumption in the park. More information and relevant figures on the flux  
231 partitioning are available in Lee et al. (2021).

## 232 **3 Results and discussion**

### 233 **3.1 Surface energy fluxes**

234 Surface energy fluxes at the SFP shows typical seasonal variations over natural forest canopies with the seasonal  
235 march of the East Asian monsoon (Fig. 4) (Hong and Kim, 2011; Hong et al., 2019b; Hong et al., 2020). There  
236 are lengthy rainy spells and large temporal variabilities of meteorological conditions during the East Asian  
237 summer monsoon period (Fig. 1d). This heavy rainfall causes substantial decreases in  $K_L$ , and thus  $Q^*$ , with large  
238 temporal variations, thereby leading to the mid-summer depression of surface fluxes (Fig. 1c and 4).  $Q^*$  also  
239 reaches its maximum in spring rather than in summer and decreases gradually from spring to winter (Fig. 4). The  
240 annual ration of  $Q_E$  to  $Q^*$  at the SFP is smaller than its global average of 0.55 and values over forest canopies at  
241 similar latitudes in the East Asia (Falge et al., 2001; Suyker and Verma, 2008; Khatun et al., 2011). In summer,  
242 about 50% of  $Q^*$  is partitioned to  $Q_E$ , and  $Q_H$  is minimum because of the ample water supply from the summer

243 rainfall.  $Q_H$  is maximum in spring and even larger in winter, despite the relatively smaller  $Q^*$ , because of the cold  
244 and dry climatic conditions induced by the winter monsoon. Accordingly, the seasonal mean Bowen ratio ( $\beta =$   
245  $\sum Q_H / \sum Q_E$ ) ranges from near zero (summer) to approximately 4 (winter) with its daily maximum around 9 in early  
246 January 2015 (Fig. 5).  $\beta$  in the SFP is consistently lower than the high-rise, high-density residential area (i.e., the  
247 EP site) because of the ET from the vegetative canopies and the unpaved surfaces in the urban forest. Daytime  
248 Bowen ratio in summer is about 0.6, which is smaller in other urban sites but is similar to suburban sites of the  
249 similar vegetation cover mainly because of the small fraction of impervious spaces around the SFP station (Table  
250 2).

251 Surface energy fluxes also shows annual variabilities over influenced by the timing of the onset and duration of  
252 the summer monsoon, similarly to natural forest in East Asia, (Hong and Kim, 2011) (Fig. 1, 4, and 5). As  
253 discussed in Section 2.2.1, annual precipitation is much larger in the first year than in the second year because of  
254 the interannual variations in the East Asian summer monsoon activity, thereby making substantial differences in  
255 surface radiative fluxes. Furthermore,  $Q_E$  shows the difference between the first and second years of the  
256 observation, particularly by responding to such interannual variability of radiation. In the first year,  $Q_E$  is more  
257 than  $300 \text{ W m}^{-2}$  and has a relatively larger temporal variability because of the frequent rainfall events in summer,  
258 compared to the second year. However, it is notable that interannual variability of surface fluxes are relatively  
259 weaker than natural forest in this region which will be better manifested in ET and its ratio to precipitation.

260 Evapotranspiration rate, which is equivalent to  $Q_E$ , ranges from  $5 \text{ mm month}^{-1}$  in January 2015 to  $74 \text{ mm month}^{-1}$   
261 in August 2013, and the annual ET values are  $367$  and  $320 \text{ mm year}^{-1}$  in the first and second years, respectively  
262 (Fig. 1 and 5 and Table 3). The ET values correspond to 29.3% and 34.3% of the annual precipitations and 49 %  
263 and 42% of net radiation, respectively. The annual ET in the second year is smaller than that in the first year with  
264 extensive drought in the second year. The difference in ET between the two consecutive years (i.e., 48 mm) mainly  
265 occurred in summer (42 mm), especially in August (30 mm) (Fig. 5). However, the ET in the second year shows  
266 only an approximately 12% decrease, despite a substantial decrease in precipitation (26% decrease) and the similar  
267 net radiation in the second year, compared to the first year (Table 3). Although the summer monsoon provides  
268 ample water to the ecosystem, its delay and weakness result in severe drought and stress to the ecosystem in this  
269 region (Hong and Kim, 2011); however, such ecosystem stress, such as the shrinking of ET and carbon uptake,  
270 has not been extensively investigated for the urban forest. We speculate that artificial irrigation by a sprinkler  
271 mitigated ecosystem stress to a certain degree in the urban forest.

### 272 **3.2 Urban heat island intensity**

273 The influence of urban forests on summer temperature is evident in UHli. Apparently, the UHli of the SFP (UHli<sup>S</sup>  
274 hereafter) and CBD (UHli<sup>C</sup> hereafter) gradually increases after mid-afternoon and is the largest at night (Fig. 6).  
275 This diurnal pattern is consistent with previous reports in cities exposed to different geographical and climatic  
276 conditions because rural areas cool faster than urban areas (Oke et al., 2017). Additionally, UHli<sup>C</sup> is positive  
277 throughout all days ranging from 0.2–2.2 °C (i.e., warmer than rural area, GP) and is greater than UHli<sup>S</sup> by 0–  
278 1.5 °C. The reason for this stronger UHli<sup>C</sup> is that the CBD stations are in the central business district; thus, the



279 densities of buildings surrounding these stations are much higher than those surrounding the SFP station. At night  
280 (19:00–06:00),  $\text{UHI}^{\text{C}}$  and  $\text{UHI}^{\text{S}}$  are approximately 1.8 °C and 1.4 °C, respectively. The maximum UHI difference  
281 between the CBD and SFP was 0.7 °C in 2013 and 0.5 °C in 2014.

282 Around sunrise, sharp declines in the UHI are observed because the air temperature near the urban area increases  
283 relatively slowly as urban fabrics, such as asphalt, brick, and concrete, have larger heat capacities and less sky  
284 view factors than the rural areas (Oke et al., 2017). Eventually, this slow increase in the air temperature reduces  
285 the differences in  $T_{\text{air}}$  among the stations, thereby reducing the UHI. The minimum  $\text{UHI}^{\text{C}}$  values were 0.3 °C  
286 (2013) at 09:30 and 0.2 °C (2014) at 08:30, while the minimum  $\text{UHI}^{\text{S}}$  occurs at 10:30 with values of –0.1 °C  
287 (2013) and 0.0 °C (2014). This implies that the timing of the minimum UHI is delayed in the SFP compared to  
288 the CBD. Notably, when there is strong ET (i.e., the first year) and more time is required to warm the SFP surface,  
289 the urban-rural difference in thermal admittance becomes relatively small. This can be attributed to the higher  
290 thermal capacity of the wetter soil of the SFP because of artificial irrigation and the absence of impervious surfaces  
291 (Oke et al., 1991). The diurnal variations in  $\text{UHI}^{\text{S}}$  also show the interannual variability in both amplitude and  
292 steepness over the two consecutive years. Despite the similar summertime  $\text{UHI}^{\text{C}}$  for both years, the daytime  
293  $\text{UHI}^{\text{S}}$  in 2013 was approximately 0.2 °C lower than that in 2014. Notably, the summer  $Q_E$  was greater in 2013  
294 than in 2014, and this observed summertime asymmetric difference between the SFP and CBD stations was not  
295 found in the winter when ET was negligible (not shown here).

296  $\Delta T_{\text{air}}$  is always positive during the entire summer season (i.e., CBD is warmer than SD) and shows distinct impacts  
297 on magnitude and diurnal variability after the park construction (Fig. 7). This difference will be larger if we  
298 consider that the measurement height at the CBD is higher than that at the SD (Table. 1). Notably, this temperature  
299 contrast mainly occurs in the afternoon when ET is dominant. The maximum  $\Delta T_{\text{air}}$  is approximately 0.3 °C around  
300 10:00 before the park construction (Fig. 7a) and increases up to approximately 0.5 °C with its peak occurrence  
301 shifting from the morning to the afternoon (i.e., around 14:00) after the construction (Fig. 7b). This peak time in  
302 the afternoon is coincident with the time when photosynthesis and  $Q_E$  are highest. The annual mean of the  
303 maximum UHI in the SD is about 4 °C and does not change significantly after the park construction compared to  
304 the CBD regions (Hong et al., 2019a). On the contrary, the daytime maximum UHI of the SD in summer decreases  
305 after the park construction (not shown here). Our results indicate that the thermal mitigation of the urban forest is  
306 important because of the wetter soil surface of the park and subsequent increases in  $Q_E$ , compared to the  
307 impervious surfaces in urban areas. This is especially true if we consider that the SFP area was originally planned  
308 to be developed as a high-population multi-purpose building complex. Our findings emphasize that the heat  
309 mitigation of the urban forest depends on the ratio of  $Q_E$  to net radiation. Indeed, there is an evident negative  
310 relationship between daytime  $Q_E$  and air temperature differences between the SFP and CBD stations (Fig. 8). As  
311  $K_{\downarrow}$  is more partitioned to  $Q_E$ ,  $T_{\text{air}}$  of the SFP decreases more than that of the CBD, and the maximum temperature  
312 difference is observed in the summer season. The SFP is cooler than the CBD by up to 0.6 °C, but the SFP is  
313 warmer than the CBD during the winter-dormant season when ET is small. Our findings confirm that urban forests  
314 are responsible for substantial changes in the thermal environment in terms of  $Q_H$  and  $Q_E$ , as well as their related

315 air and surface temperatures because of more evaporative cooling in green spaces compared to impervious  
316 surfaces such as roads and buildings in urban areas (Oke et al., 2017).

317

### 318 3.3 Temporal dynamics of net CO<sub>2</sub> exchange

319 Overall, the mean daytime  $F_C$  is negative (i.e., carbon uptake) in the summer (June–August), indicating that  
320 photosynthesis, the only carbon sink, is dominant in the growing season (Fig. 9). This carbon uptake period is  
321 coincident with the active vegetation manifested by increases in EVI (not shown here). Summertime  
322 photosynthetic carbon uptake ( $GPP$ ) has a daily average of  $7.6 \mu\text{mol m}^{-2} \text{s}^{-1}$  with a maximum of  $18.9 \mu\text{mol m}^{-2} \text{s}^{-1}$   
323 around 12:30 (Fig. 9 and 10). A daily minimum  $F_C$  also occurs around 12:30 with the maximum photosynthetic  
324 carbon uptake during this time. CO<sub>2</sub> uptake is highest in June, with a maximum of approximately  $13 \mu\text{mol m}^{-2} \text{s}^{-1}$   
325 (Fig. 9a). In the middle of summer (4th and 31st two-week data in Fig. 9a), CO<sub>2</sub> uptake decreases significantly  
326 because photosynthesis is limited because of the reduced  $K_{\downarrow}$  by cloud and rainfall with the onset of the summer  
327 monsoon (Fig. 1c). This mid-summer depression of carbon uptake has been reported in the Asian natural  
328 vegetations (e.g., Kwon et al., 2009; Hong and Kim, 2011; Hong et al., 2014). Greater reduction in CO<sub>2</sub> uptake  
329 observed in 2013 than in 2014 was attributed to a longer monsoon period in 2013. Indeed, from 8 to 21 July 2013  
330 (4th two-week data in Fig. 9a), the accumulated precipitation was approximately 400 mm for two weeks, and the  
331 daily averaged  $K_{\downarrow}$  was only  $70 \text{ W m}^{-2}$ .

332 The vegetation around the SFP absorbs more CO<sub>2</sub> than is emitted by local carbon sources and  $F_C$  is negative only  
333 during the summer daytime. Because of substantial amounts of anthropogenic emissions and ecosystem  
334 respiration,  $F_C$  changes from negative (i.e., carbon sink) to positive values (i.e., carbon source) even around 16:30  
335 in summer unlike in natural ecosystems, despite the substantial downward shortwave (e.g., Desai et al., 2008;  
336 Hong et al., 2009; Alekseychik et al., 2017; Chatterjee et al., 2020). As photosynthesis decreases,  $F_C$  changes to  
337 positive values from November. During the non-growing season (i.e., late autumn, winter, and early spring),  
338 anthropogenic emissions were also dominant because photosynthesis and ecosystem respiration decrease with  
339 smaller  $K_{\downarrow}$  and lower temperatures. During these periods,  $F_C$  had minimum values at 04:00–05:00 and increases  
340 until 15:00–16:00. The diurnal variations in  $F_C$  mainly followed the traffic volume. There also is a clear positive  
341 relationship between  $F_C$  and  $\lambda$  (Fig. 4 in Lee et al., 2021). It is also noteworthy that the peak time of  $F_C$  (16:00) is  
342 earlier than the peak time of  $\lambda$  (18:00) from December to early March because  $E_B$  is the largest at around 15:00–  
343 16:00, indicating that  $E_R$  and  $E_B$  are the controlling factor of  $F_C$  in this period.

344 The seasonal  $F_C$  variation also depends on the spatio-temporal distribution of CO<sub>2</sub> sources and flux footprint  
345 because the latter covers various land use with changes in wind direction and atmospheric stability (Fig. 10). In  
346 autumn, the main wind direction changes to the north as the synoptic conditions change as discussed in section 2  
347 (Fig. 2); therefore,  $\lambda$  is smaller in autumn compared to other seasons (Fig. 9b). For example, the road fraction is  
348 smallest at < 1% from midnight to midday and < 3% during the afternoon in October and November (11th, 12th,  
349 36th, and 37th two-week data in Fig. 9b). In these periods, the nighttime  $F_C$  shows the lowest value of

350 approximately  $2.9 \mu\text{mol m}^{-2} \text{s}^{-1}$ , which is attributable to the smallest road fraction, lower respiration, and minimal  
351 heating usage.

352 In early spring,  $\lambda$  is generally larger; thus,  $E_R$  plays a significant role in  $F_C$ , and  $E_B$  remains non-zero until early  
353 April because of anthropogenic emission by hot water and space heating in the building within the footprint,  
354 thereby resulting in the largest  $F_C$  in this period. With a shutdown of the heating system (i.e., zero  $E_B$ ) and the  
355 sprouting of leaves in April, there is a sharp decrease in  $F_C$  (Fig. 10c). From December to March,  $\text{CO}_2$  emissions  
356 increase up to  $30 \mu\text{mol m}^{-2} \text{s}^{-1}$  with larger variability because of intermittent anthropogenic emissions from the  
357 park facility building in the south-west directions (due to space heating and boiling water), as well as the relatively  
358 increased contribution of vehicles on the road in the western part of the site (Fig. 10b).

359 Although the positive  $F_C$  in the winter decreases in spring, its magnitude shows directional differences (Fig. 10c).  
360 On the eastern side, the mean  $F_C$  shows a negative value in May, whereas it remains positive on the western side  
361 ( $210\text{--}270^\circ$ ) until May. These findings further indicate the different contributions of various carbon sources and  
362 sinks among the different wind directions. For the wind directions from the north to the east ( $0\text{--}120^\circ$ ),  $F_C$  shows  
363 a relatively weaker carbon sink than other directions because of the relatively low tree fraction in this direction  
364 (Fig. 10a and 10c). On the southern side ( $150\text{--}180^\circ$ ) having the highest tree cover fraction, a maximum carbon  
365 uptake is about  $15 \mu\text{mol m}^{-2} \text{s}^{-1}$  in June. However, despite the dense vegetation on the south and west side ( $120\text{--}$   
366  $330^\circ$ ), the  $F_C$  magnitude was much smaller than that of other natural forests. This is related to the anthropogenic  
367 emissions from vehicles on the roads which is discussed in section 3.5.

### 368 **3.4 Light use efficiency of biogenic $\text{CO}_2$ components**

369  $F_C$  at the SFP shows a typical light response to the photosynthetically active radiation (PAR) in a way similar to  
370 natural ecosystems in spite of anthropogenic  $\text{CO}_2$  sources from vehicles (Fig. 11). However, this light response in  
371 the urban forest is a distinct contrast to  $F_C$  in high-rise high-population residential areas in Seoul under the same  
372 climatic conditions that does not respond to PAR (i.e., EP station). Importantly,  $GPP$ ,  $NBE$ , and  $F_C$  show different  
373 trends on PAR depending on the direction. As stated in Section 2.2.2 and 3.3, the western side has a higher density  
374 of trees as against more grass on the eastern side, and biotic  $\text{CO}_2$  uptake from the western side is substantially  
375 larger than that on the eastern side. Accordingly, the slope of the light response curve for PAR on the western side  
376 is steeper than on the eastern side.  $F_C$  at zero PAR ( $F_{C,0}$ ) is larger on the western side ( $9.7 \mu\text{mol m}^{-2} \text{s}^{-1}$ ) than on  
377 the eastern side ( $5.1 \mu\text{mol m}^{-2} \text{s}^{-1}$ ) because of a contribution of  $E_R$  from roads on the western side of the tower.

378  $NBE$  shows a comparable light response to natural vegetation (e.g., Schmid et al., 2003). A rectangular hyperbolic  
379 equation has been used to examine the light response of  $NBE$  and elucidate the directional differences in carbon  
380 uptake:

$$381 \quad NBE = -GPP + RE = -\frac{\alpha \cdot GPP_{sat} \cdot PAR}{GPP_{sat} + \alpha \cdot PAR} + RE \quad (3)$$

382  $\alpha$  is approximately  $0.0651$  and  $0.0558 \mu\text{mol CO}_2 (\mu\text{mol photon})^{-1}$  on the western and eastern sides, respectively.  
383 Notably,  $\alpha$  on the western side is comparable to the high initial quantum yield in crops and subtropical forests in

384 East Asia (Hong et al., 2019b; Emmel et al., 2020). Additionally,  $GPP_{sat}$  is 30.9 and 12.7  $\mu\text{mol m}^{-2} \text{s}^{-1}$  on the  
385 western and eastern sides, respectively. In addition, the light saturation points are at a PAR of 1500  $\mu\text{mol m}^{-2} \text{s}^{-1}$   
386 on the eastern side, which occur at a relatively lower PAR than on the western side. Daytime respiration estimates  
387 from equation (3) is 6.7 and 6.3  $\mu\text{mol m}^{-2} \text{s}^{-1}$  on the western and eastern sides, respectively. Because  $GPP$  is related  
388 to PAR, the difference in monthly cumulative  $GPP$  between the two years shows a close relationship with the  
389 difference in the monthly sunshine duration ( $r^2 = 0.75$ , not shown here), suggesting a possible impact of change  
390 in the onset of the summer monsoon on urban forests.

391 The magnitude of  $NBE$  from the western side is larger than that from a suburban area with about 50% vegetative  
392 fraction in Montreal, Canada (Fig. 7b in Bergeron and Strachan, 2011) and  $F_C$  from a highly vegetated  
393 environment of about 67% vegetative fraction in Baltimore, USA (Crawford et al., 2011). Also,  $GPP$  from the  
394 western side is comparable to the dense forest canopies in subtropical forests in Korea (Hong et al., 2019b),  
395 deciduous forest ecosystems (Goulden et al., 1996), and a mixed hardwood forest ecosystem (Schmid et al., 2000).  
396 However,  $NBE$  from the eastern side is similar to  $F_C$  from the suburban areas of about 44%, 50%, and 64%  
397 vegetative fraction in Swindon, UK (Ward et al., 2013) and Montreal, Canada (Bergeron and Strachan, 2011), and  
398 Ochang, Korea in the same climate zone (Hong et al., 2019b), respectively.

### 399 **3.5 Annual budget of CO<sub>2</sub> sources and sink**

400 The annual sums of the  $GPP$  and  $RE$  in the SFP are 4.6 kg CO<sub>2</sub> m<sup>-2</sup> year<sup>-1</sup> (1244 gC m<sup>-2</sup> year<sup>-1</sup>) and 5.1 kg CO<sub>2</sub> m<sup>-2</sup>  
401 year<sup>-1</sup> (1378 gC m<sup>-2</sup> year<sup>-1</sup>), respectively (Table 4). This photosynthetic carbon uptake is smaller than its global  
402 mean  $GPP$  in natural deciduous broadleaf forests with similar annual precipitation and annual mean air  
403 temperature (total 8 years of data from 4 sites of FLUXNET2015 dataset reported in Pastorello et al., 2020) and  
404 similar to that of deciduous broadleaf forests in East Asia (Awal et al., 2010; Kwon et al., 2010) (Table 5).  
405 However, we note that this  $GPP$  is relatively larger if we consider the low vegetation fraction and leaf area index  
406 (LAI) at our urban park. Previous studies have shown that the  $GPP$  of urban vegetation is scaled with vegetation  
407 cover fraction with an increase of about 0.7 kg CO<sub>2</sub> m<sup>-2</sup> year<sup>-1</sup> per 10% increase in vegetation cover fraction (Awal  
408 et al., 2010; Crawford and Christen, 2015; Velasco et al., 2016; Menzer and McFadden, 2017). Indeed,  $GPP$  at  
409 the SFP with a 46.6% vegetation cover fraction is approximately 1.5 kg CO<sub>2</sub> m<sup>-2</sup> year<sup>-1</sup> which is larger than values  
410 reported in other urban sites if it is scaled with the vegetation cover fraction (Fig. 12a).

411 Despite this larger  $GPP$  resulting smaller  $F_C$  eventually, there is no substantial decrease in  $F_C$  when they are scaled  
412 by vegetation fraction, suggesting large contribution of  $RE$  (Fig. 12b). There was a linear decrease in  $F_C$  of  
413 approximately 3.0 kg CO<sub>2</sub> m<sup>-2</sup> year<sup>-1</sup> per 10% increase in vegetation cover fraction based on the observed  $F_C$   
414 across an urbanization gradient (Hong et al., 2019b and references therein). The annual  $F_C$  in the SFP is not so  
415 much different from other similar cities and this scaled relationship. Meanwhile,  $RE$  at our site is much larger than  
416 that in natural temperate deciduous forests in the similar climate zone (Takanashi et al., 2005; Kwon et al., 2010)  
417 and similar to that in the urban forest in East Asia (Awal et al., 2010), as well as to the global mean  $RE$  over forests  
418 with similar annual precipitation and annual mean air temperatures (Pastorello et al., 2020). Put differently, the  
419 urban forest considered in our study is an outlier compared to other natural forest canopies and urban forests

420 because  $RE/GPP > 1$  (Table 5). Autotrophic respiration is considered to be approximately half of GPP as a rule  
421 of thumb (Piao et al., 2010), which corresponds to approximately 45% of the RE at our site, thereby indicating a  
422 large contribution of heterotrophic respiration to RE. Indeed, it was reported that soil respiration at the same site  
423 was approximately  $4 \text{ kg CO}_2 \text{ m}^{-2} \text{ year}^{-1}$  (Bae and Ryu, 2017). The reason for the large soil organic carbon was  
424 mainly because rice cultivation was carried out in this region before the 1950s, and organic carbon-rich soil was  
425 transplanted during the SFP construction, and fertilizers were applied regularly. It has also been reported that RE  
426 is enhanced in urban areas because of the relatively warmer temperature in urban regions (i.e., UHI) (Awal et al.,  
427 2010). Notably,  $Q_{10}$  (the rate by which respiration is multiplied when temperature increases by  $10 \text{ }^\circ\text{C}$ ) is about 1.9  
428 at the site and matches the  $Q_{10}$  value for ecosystem respiration ( $2.2 \pm 0.7$ ) calculated for natural forests across 42  
429 FLUXNET sites (Mahecha et al., 2010). Further analysis based on the observed  $Q_{10}$  and the UHI at the SFP  
430 indicates that UHI leads to an approximately 5% increase in RE.

431 Seasonal variations in the strength of carbon sources and sink as well as  $F_C$  are mainly regulated by the biogenic  
432 component in summer and the anthropogenic component in winter (Fig. 13). Furthermore,  $F_C$  is minimum in June,  
433 despite the similar GPP from June to August because of the relatively smaller RE during the summer season. Even  
434 in summer, photosynthetic carbon uptake is balanced with ecosystem respiration and does not offset all biotic and  
435 anthropogenic emissions, thus resulting in positive  $F_C$  values throughout the year. In winter,  $E_B$  is dominant with  
436 negligible GPP and RE due to cold temperatures, and  $E_R$  also becomes larger than RE from November.  $E_R$  shows  
437 apparent seasonal variation in wind direction and atmospheric stability. Its magnitude is about  $0.0666 \mu\text{mol m}^{-2}$   
438  $\text{veh}^{-1} \text{ h}^{-1}$  in neutral condition and consistent with the value in the inventory data (Lee et al., 2021). The average  
439 monthly traffic speed for the road in front of the SFP is  $50\text{--}60 \text{ km h}^{-1}$  (based on the January 2014 data from the  
440 Seoul Metropolitan Government Traffic Speed Report), and the  $\text{CO}_2$  emission rate is approximately  $150 \text{ g CO}_2$   
441  $\text{km}^{-1} \text{ veh}^{-1}$  based on the emission data at this speed (Kim et al., 2011). With the width of the ten-lane road ( $25\text{--}$   
442  $30 \text{ m}$ ), the inventory-based slope (i.e.,  $\text{CO}_2$  emission rate per vehicle per area per half-hour) is approximately in  
443 the range of  $0.0631\text{--}0.0757 \mu\text{mol m}^{-2} \text{ veh}^{-1} \text{ half-hour s}^{-1}$  ( $\cong 150 \text{ gCO}_2 \text{ km}^{-1} \text{ veh}^{-1} \times 1/30$  or  $1/25 \text{ m}^{-1} \times 1/44 \text{ mol}$   
444  $\text{gCO}_2^{-1} \times 10^{-3} \text{ km m}^{-1} \times 10^6 \mu\text{mol mol}^{-1} \times 1/1800 \text{ half-hour s}^{-1}$ ).

445 There is an evident yearly difference in individual carbon sources and sink in two consecutive years.  $E_B$  is mainly  
446 caused by heating buildings and hot water in park facilities using natural gas. Notably,  $E_B$  is highly correlated with  
447 gas consumption in SFP during winter on monthly basis ( $R^2 = 0.94$ ; Fig. 6 in Lee et al., 2021).  $E_B$  is smaller in the  
448 first year because of the relatively smaller number of park visitors and consequently smaller gas consumption,  
449 compared to the second year. Eventually, these annual differences lead to a smaller annual mean total  $F_C$  in the  
450 first year than in the second year (Table 4). RE is maximum in the August of the first year, while it is highest in  
451 July in the second year because the monthly mean air temperature is highest in August of the first and July of the  
452 second year with annual variations in air temperature with changes in the timing and duration of the East Asian  
453 summer monsoon, of which impacts have also been reported in natural vegetation in the same region (Hong and  
454 Kim, 2011; Hong et al., 2019b). GPP in summer is relatively smaller in the first year by the mid-summer  
455 depression of solar radiation because of the elongated monsoon period but annual sums of GPP are similar in two  
456 years (Table 4 and Fig. 13). GPP does not shrink in the second year of significant drought because of ample water

457 supply by a sprinkler. Eventually,  $F_C$  in the SFP is approximately  $3.0 \text{ kg CO}_2 \text{ m}^{-2} \text{ year}^{-1}$  less than that in recently  
458 developed high-rise high-population urban areas in Seoul. Our results suggest that efficient management of urban  
459 forests, such as regular irrigation and fertilization, can be an efficient way to adapt and mitigate climate change  
460 by increasing  $\text{CO}_2$  uptake in artificial forest constructions in East Asia.

#### 461 **4 Summary and conclusions**

462 This study reported two-year surface fluxes of energy and  $\text{CO}_2$  measured by the eddy covariance method in order  
463 to examine the role of artificially generated urban forests in mitigating air temperature and anthropogenic  $\text{CO}_2$   
464 emissions. The study area is an urban park with an artificially planted forest in the Seoul Metropolitan Area  
465 redeveloped from a racetrack and factory in the mid-2000s where is influenced by a lengthy summer rainy season  
466 during the East Asian summer monsoon. To examine the mitigation of air temperature, this study compares  
467 meteorological conditions in the urban forest with the surrounding high-rise high-population urban areas. This  
468 study applies for the ANN-based gap filling and a statistical  $\text{CO}_2$  flux partitioning method based on temporal  
469 subsets of flux data and high-resolution footprint-weighted land use data to understand the abiotic and biotic  
470 contributions to  $F_C$ .

471 Surface energy fluxes in the SFP is influenced by the summer monsoon, and more energy is distributed to  $Q_E$  than  
472  $Q_H$  in the summer in the growing season, similarly to natural forests in this climate zone. The Bowen ratio in this  
473 urban forest ranges from near 0 (summer) to about 4 (winter), which is lower throughout the year than that of  
474 high-rise and high-density residential areas in Seoul. This suggests that the vegetation and unpaved surfaces of  
475 urban forests facilitate more evaporative cooling compared to the impervious surfaces in urban areas. During the  
476 measurement period, the second year is contrasted with the first year because of the drought compared to the  
477 normal climate condition in the first year. Notably, ET decreases in the second year, but this drop is not as much  
478 as the reduced precipitation and its related changes in radiative forcing during the drought because of the artificial  
479 irrigation by a sprinkler mitigated ecosystem.

480 It is also evident that the urban forest reduced the warming trend and UHI around the study area. Air temperature  
481 in the SFP is lower than the surrounding area, but this coolness is reinforced after the park was created. The  
482 warming trend diminishes after the construction of the park and is smaller than that in other urban regions in the  
483 Seoul Metropolitan Area. In addition, the construction of the park delays the timing of the maximum temperature  
484 difference between the urban forest and high-rise commercial from the morning to the afternoon, coinciding with  
485 the timing of the maximum  $Q_E$ . The SFP shows a typical diurnal UHI variation pattern, which has a higher  
486 temperature at night than in rural areas. However, the UHI in SFP is lower by  $0.6 \text{ }^\circ\text{C}$  in summer compared to the  
487 surrounding urban area, and the time of the minimum peak time is delayed, possibly because vegetation and  
488 permeable soils in SFP have a larger thermal capacity. Notably, UHI decreases more in the partitioning of  
489 incoming energy into latent heat fluxes and there was cooling by  $0.2 \text{ }^\circ\text{C}$  compared to the surrounding urban area  
490 if  $Q_E/K_1$  increased by 10% in this study.

491 Net CO<sub>2</sub> exchange at the urban forest shows typical temporal variations in natural forest canopies influenced by  
492 the East Asian summer monsoon. A mid-summer depression of carbon uptake is observed with the onset of the  
493 summer monsoon, like vegetation in the East Asian monsoon region. The *GPP* is estimated by the statistical  
494 partitioning method, and the non-zero *GPP* period is coincident with the active vegetation of the significant  
495 vegetation index. Summertime photosynthetic carbon uptake has a daily average of 7.6  $\mu\text{mol m}^{-2} \text{s}^{-1}$  with a  
496 maximum of 18.9  $\mu\text{mol m}^{-2} \text{s}^{-1}$  around 12:30. However, even during the growing season, vegetative carbon uptake  
497 is insufficient to offset anthropogenic CO<sub>2</sub> emissions and ecosystem respiration on a time scale of > 1 day. Our  
498 estimations of anthropogenic CO<sub>2</sub> emissions from vehicles and buildings agree with the estimations based on  
499 inventory data such as CO<sub>2</sub> emission rate of vehicles and monthly gas consumption, and their annual budgets each  
500 have a comparable magnitude to *GPP*.

501 Annual *GPP* of the urban forest is relatively smaller than that of the forest in East Asia exposed to similar climatic  
502 conditions because of the relatively smaller vegetation cover fraction and LAI. However, it is larger than the *GPP*  
503 expected from the relationship from previous urban studies if it is normalized by the vegetation cover fraction.  
504 *RE* is, however, much larger than that in the temperate East Asian forests and is similar to the urban forest in East  
505 Asia. We speculate that soil respiration enhances such large *RE* by relatively warmer temperatures in a city and  
506 rich soil organic carbon in the SFP. The annual mean total *FC* is 7.1 kg CO<sub>2</sub> m<sup>-2</sup> year<sup>-1</sup>, which is smaller than the  
507 estimate from the scaling between annual total *FC* and vegetation fraction (Hong et al., 2019b). Because of the  
508 spatial heterogeneity, *FC* and its components showed directional changes. *NBE* from the eastern side is similar to  
509 that in suburban areas with approximately 44%, 50%, and 64% vegetative fraction in Swindon, UK (Ward et al.,  
510 2013) and Montreal, Canada (Bergeron and Strachan, 2011), and Ochang, Korea in the same climate zone (Hong  
511 et al., 2019b), respectively. However, the *NBE* and *GPP* from the western side are comparable to dense forest  
512 canopies in subtropical forests in Korea (Hong et al., 2019b), deciduous forest ecosystems (Goulden et al., 1996),  
513 and a mixed hardwood forest ecosystem (Schmid et al., 2000).

514 Our results emphasize the important role of forest management in enhancing carbon uptake and evaporative  
515 cooling despite the low vegetation fraction. Our key findings are that urban forests in East Asia are highly  
516 influenced by the East Asian monsoon like natural forests in this region, but such influence is mitigated by  
517 artificial irrigation and fertilization in urban forests. Our results emphasize the importance of forest management  
518 for efficient carbon uptake and evaporative cooling despite the low vegetation fraction. Furthermore, our  
519 observation study also indicates that caution in soil management is necessary to reduce CO<sub>2</sub> emissions in urban  
520 forests, mainly resulting from large soil organic carbon and warm environment.

521

522 *Acknowledgment.* This research was supported by the Korea Meteorological Administration Research and  
523 Development Program under Grant KMI2021-01610 and National Research Foundation of Korea Grant from the  
524 Korean Government (MSIT) (NRF-2018R1A5A1024958). All data and codes are available in Lee et al. (2021)  
525 and upon request to the corresponding author (jhong@yonsei.ac.kr / <https://eapl.yonsei.ac.kr>).

526





<b>Abbreviation</b>	<b>Definitions</b>	<b>Abbreviation</b>	<b>Definitions</b>
CBD	the Gangnam, Seocho, and Songpa observatories at central business district	RE	ecosystem respiration
$E_B$	CO <sub>2</sub> emission from buildings	SD	the Seongdong weather station
EC	eddy covariance	SEB	surface energy balance
EP	the Eunpyeong site	SFP	the Seoul Forest Park
$E_R$	CO <sub>2</sub> emission from vehicles on roads	$T_{air}$	the screen-level air temperature
ET	evapotranspiration	$T_{air\_CBD}$	air temperature at the CBD regions
EVI	enhanced vegetation index	$T_{air\_SD}$	air temperature at the SD
$F_C$	net CO <sub>2</sub> exchange	UHI	urban heat island
$F_{C_0}$	$F_C$ at zero <i>PAR</i>	UHI <sub>i</sub>	urban heat island intensity
GP	the Gimpo weather station	UHI <sub>i</sub> <sup>C</sup>	UHI <sub>i</sub> at CBD
<i>GPP</i>	gross primary production	UHI <sub>i</sub> <sup>S</sup>	UHI <sub>i</sub> at SFP
$GPP_{sat}$	potential rate of ecosystem CO <sub>2</sub> uptake	VPD	vapor pressure deficit
$K_{\downarrow}$	downward shortwave radiation	$\Delta T_{air}$	$T_{air\_CBD} - T_{air\_SD}$
LCZ	local climate zone	$\Delta Q_S$	the net storage heat flux
MAP	mean annual precipitation	$\Delta Q_A$	the net heat advection
MAT	mean annual temperature	$h_c$	mean canopy height
NBE	net biome exchange of CO <sub>2</sub> ( $RE - GPP$ )	$z_0$	mean roughness length
P	precipitation	$z_d$	zero-plane displacement height
PAR	photosynthetic active radiation	$z_m$	measurement height
$Q_E$	latent heat flux	$\alpha$	quantum yield efficiency
$Q_F$	anthropogenic heat flux	$\beta$	Bowen ratio ( $= \Sigma Q_H / \Sigma Q_E$ )

$Q_H$	sensible heat flux	$\lambda$	source area weighted road ratio
$Q^*$	net radiation	$\lambda_v$	Vegetation cover fraction
$Q_{10}$	the rate by which respiration is multiplied when temperature increases by 10°C		

529

530 **References**

- 531 Alekseychik, P., Mammarella, I., Karpov, D., Dengel, S., Terentieva, I., Sabrekov, A., Glagolev, M. and Lapshina,  
532 E.: Net ecosystem exchange and energy fluxes measured with the eddy covariance technique in a western Siberian  
533 bog. *Atmospheric Chemistry and Physics*, 17, 9333-9345, 2017.
- 534 Awal M. A, Ohta T., Matsumoto K., Toba T., Daikoku K., Hattori S., and coauthors: Comparing the carbon  
535 sequestration capacity of temperate deciduous forests between urban and rural landscapes in central Japan. *Urban*  
536 *Forestry & Urban Greening*, 9(3), 261-270, 2010.
- 537 Bae, J., and Ryu, Y.: Spatial and temporal variations in soil respiration among different land cover types under  
538 wet and dry years in an urban park. *Landscape and Urban Planning*, 167, 378–385, 2017.
- 539 Ballinas, M., and Barradas, V. L.: The urban tree as a tool to mitigate the urban heat island in Mexico City: A  
540 simple phenomenological model. *Journal of environmental quality*, 45(1), 157-166, 2016.
- 541 Balogun, A. A., Adegoke, J. O., Vezhapparambu, S., Mauder, M., McFadden, J. P. and Gallo, K.: Surface energy  
542 balance measurements above an exurban residential neighbourhood of Kansas City, Missouri. *Boundary-Layer*  
543 *Meteorology*. 133, 299-321, 2009.
- 544 Bergeron, O., and Strachan, I. B.: CO<sub>2</sub> sources and sinks in urban and suburban areas of a northern mid-latitude  
545 city. *Atmospheric Environment*, 45(8), 1564-1573, 2011.
- 546 Bonan, G. B.: Forests and climate change: forcings, feedbacks, and the climate benefits of forests. *Science*, 320,  
547 1444-1449. 2008.
- 548 Bowler, D. E., Buyung-Ali, L., Knight, T. M., and Pullin, A. S.: Urban greening to cool towns and cities: A  
549 systematic review of the empirical evidence. *Landscape and Urban Planning*, 97(3), 147-155, 2010.
- 550 Chang, C. R., Li, M. H., and Chang, S. D.: A preliminary study on the local cool-island intensity of Taipei city  
551 parks. *Landscape and Urban Planning*, 80(4), 386-395, 2007.
- 552 Chatterjee, S., Swain, C.K., Nayak, A.K., Chatterjee, D., Bhattacharyya, P., Mahapatra, S.S., Debnath, M.,  
553 Tripathi, R., Guru, P.K. and Dhal, B.: Partitioning of eddy covariance-measured net ecosystem exchange of CO<sub>2</sub>  
554 in tropical lowland paddy. *Paddy and Water Environment*, 18, 623-636, 2020.
- 555 Chiesura, A.: The role of urban parks for the sustainable city. *Landscape and Urban Planning*, 68(1), 129-138,  
556 2004.
- 557 Christen, A.: Atmospheric measurement techniques to quantify greenhouse gas emissions from cities. *Urban*  
558 *Climate*, 10, 241-260, 2014.
- 559 Christen, A. and Vogt, R.: Energy and radiation balance of a central European city. *International Journal of*  
560 *Climatology*. 24, 1395-1421, 2004.
- 561 Coutts, A. M., Beringer, J., and Tapper, N. J.: Impact of increasing urban density on local climate: Spatial and  
562 temporal variations in the surface energy balance in Melbourne, Australia. *Journal of Applied Meteorology and*  
563 *Climatology*. 46(4), 477-493, 2007a.
- 564 Coutts, A. M., Beringer, J., and Tapper, N. J.: Characteristics influencing the variability of urban CO<sub>2</sub> fluxes in  
565 Melbourne, Australia. *Atmospheric Environment*, 41(1), 51-62, 2007b.
- 566 Crawford, B., Grimmond, C. S. B., and Christen, A.: Five years of carbon dioxide fluxes measurements in a highly  
567 vegetated suburban area. *Atmospheric Environment*, 45(4), 896-905, 2011.

568 Crawford, B., and Christen, A.: Spatial source attribution of measured urban eddy covariance CO<sub>2</sub> fluxes.  
569 *Theoretical and Applied Climatology*, 119(3-4), 733-755, 2015.

570 Desai, A.R., Richardson, A.D., Moffat, A.M., Kattge, J., Hollinger, D.Y., Barr, A., Falge, E., Noormets, A., Papale,  
571 D., Reichstein, M. and Stauch, V.J.: Cross-site evaluation of eddy covariance GPP and RE decomposition  
572 techniques. *Agricultural and Forest Meteorology*, 148, 821-838, 2008.

573

574 Emmel, C., D'Odorico, P., Reville, A., Hörtnagl, L., Ammann, C., Buchmann, N. and Eugster, W.: Canopy  
575 photosynthesis of six major arable crops is enhanced under diffuse light due to canopy architecture. *Global Change  
576 Biology*, 26(9), 2020.

577 Falge, E., Baldocchi, D., Olson, R., Anthoni, P., Aubinet, M., Bernhofer, C., Burba, G., Ceulemans, R., Clement,  
578 R., Dolman, H., Granier, A., Gross, P., Grünwald, T., Hollinger, D., Jensen, N., Katul, G., Keronen, P., Kwalski,  
579 A., Lai, C., Law, B., Meyers, T., Moncrieff, J., Moors, E., Munger, W., Pilegaard, K., Rannik, Ü., Rebmann, C.,  
580 Suyker, A., Tenhunen, J., Tu, K., Verma, S., Vesala, T., Wilson, K., and Wofsy, S.: Gap filling strategies for long  
581 term energy flux data sets. *Agricultural and Forest Meteorology*, 107, 71-77, 2001.

582 Feigenwinter, C., Vogt, R., and Christen, A.: Eddy covariance measurements over urban areas. In *Eddy  
583 Covariance* (pp. 377-397). Springer, Dordrecht, 2012.

584 Feyisa, G. L., Dons, K., and Meilby, H.: Efficiency of parks in mitigating urban heat island effect: An example  
585 from Addis Ababa. *Landscape and Urban Planning*, 123, 87-95, 2014.

586 Goldbach, A. and Kuttler, W.: Quantification of turbulent heat fluxes for adaptation strategies within urban  
587 planning. *International Journal of Climatology*, 33, 143-159, 2013.

588 Goulden, M. L., Munger, J. W., Fan, S. M., Daube, B. C., and Wofsy, S. C.: Measurements of carbon sequestration  
589 by long-term eddy covariance: Methods and a critical evaluation of accuracy. *Global Change Biology*, 2(3), 169-  
590 182, 1996.

591 Grimmond, C. S. B. and Oke, T. R.: Comparison of heat fluxes from summertime observations in the suburbs of  
592 four North American cities. *Journal of Applied Meteorology*, 34, 873-889, 1995.

593 Grimmond, C. S. B. and Oke, T. R.: Aerodynamic properties of urban areas derived from analysis of surface form.  
594 *Journal of Applied Meteorology and Climatology*, 38, 1262-1292, 1999.

595 Haaland, C., and van Den Bosch, C. K.: Challenges and strategies for urban green-space planning in cities  
596 undergoing densification: A review. *Urban forestry & Urban Greening*, 14(4), 760-771, 2015.

597 Hamada, S., and Ohta, T.: Seasonal variations in the cooling effect of urban green areas on surrounding urban  
598 areas. *Urban Forestry & Urban Greening*, 9(1), 15-24, 2010.

599 Hansen, J., Ruedy, R., Sato, M., and Lo, K.: Global surface temperature change. *Reviews of Geophysics*, 48(4),  
600 2010.

601 Hiller, R. V., McFadden, J. P., and Kljun, N.: Interpreting CO<sub>2</sub> fluxes over a suburban lawn: the influence of  
602 traffic emissions. *Boundary-Layer Meteorology*, 138(2), 215-230, 2011.

603 Hong, J., and Kim, J.: Impact of the Asian monsoon climate on ecosystem carbon and water exchanges: a wavelet  
604 analysis and its ecosystem modeling implications. *Global Change Biology*, 17(5), 1900-1916, 2011.

605 Hong, J., Kwon, H., Lim, J., Byun, Y., Lee, J., and Kim, J.: Standardization of KoFlux eddy-covariance data  
606 processing. *Korean J. Agric. For. Meteorol.*, 11, 19-26, 2009.

607 Hong, J., Takagi, K., Ohta, T., and Kodama, Y.: Wet surface resistance of forest canopy in monsoon Asia:  
608 Implications for eddy-covariance measurement of evapotranspiration. *Hydrological Processes*, 28(1), 37-42, 2014.

609 Hong, J. W., Hong, J., Lee, S. E., and Lee, J.: Spatial distribution of urban heat island based on local climate zone  
610 of automatic weather station in Seoul metropolitan area. *Atmosphere*, 23(4), 413-424, 2013.

611 Hong, J. W., and Hong, J.: Changes in the Seoul metropolitan area urban heat environment with residential  
612 redevelopment. *Journal of Applied Meteorology and Climatology*, 55(5), 1091-1106, 2016.

613 Hong, J. W., Hong, J., Kwon, E. E., and Yoon, D.: Temporal dynamics of urban heat island correlated with the  
614 socio-economic development over the past half-century in Seoul, Korea. *Environmental Pollution*, 254, 112934,  
615 2019a.

616 Hong, J.-W., Hong, J., Chun, J., Lee, Y., Chang, L., Lee, J., Yi, K., Park, Y., Byun, B., and Joo, S.: Comparative  
617 assessment of net CO<sub>2</sub> exchange across an urbanization gradient in Korea based on in situ observation, *Carbon*  
618 *Balance and Management*, <https://doi.org/10.1186/s13021-019-0128-6>, 2019b.

619 Hong, J. W., Lee, S. D., Lee, K., and Hong, J.: Seasonal variations in the surface energy and CO<sub>2</sub> flux over a high-  
620 rise, high-population, residential urban area in the East Asian monsoon region. *International Journal of*  
621 *Climatology*, <https://doi.org/10.1002/joc.6463>, 2020.

622

623 Hsieh, C. I., Katul, G., and Chi, T. W.: An approximate analytical model for footprint estimation of scalar fluxes  
624 in thermally stratified atmospheric flows. *Advances in Water Resources*, 23(7), 765-772, 2000.

625 Kennedy, C. A., Ibrahim, N., and Hoornweg, D.: Low-carbon infrastructure strategies for cities. *Nature Climate*  
626 *Change*, 4(5), 343, 2014.

627 Kent, C. W., Lee, K., Ward, H. C., Hong, J. W., Hong, J., Gatey, D., and Grimmond, S.: Aerodynamic roughness  
628 variation with vegetation: analysis in a suburban neighbourhood and a city park. *Urban Ecosystems*, 21(2), 227-  
629 243, 2018.

630 Khatun, R., Ohta, T., Kotani, A., Asanuma, J., Gamo, M., Han, S., Hirano, T., Nakai, Y., Saigusa, N., Takagi, K.  
631 and Wang, H. (2011) Spatial variations in evapotranspiration over East Asian forest sites. I. Evapotranspiration  
632 and decoupling coefficient. *Hydrological Research Letters*, 5, 83-87, 2011.

633 Kim, Y., Woo, S.K., Park, S., Kim, M. and Han, D.: A Study on Evaluation Methodology of Greenhouse Gas and  
634 Air Pollutant Emissions on Road Network - Focusing on Evaluation Methodology of CO<sub>2</sub> and NO<sub>x</sub> Emissions  
635 from Road. Korea: The Korea Transport Institute (Annual Report), 2011.

636 Kirschbaum, M.U.F., Eamus, D., Gifford, R.M., Roxburgh, S.H. and Sands, P.J.: Definitions of some ecological  
637 terms commonly used in carbon accounting. In *Net Ecosystem Exchange Workshop*, 18-20, 2001.

638 Kroeger, T., McDonald, R. I., Boucher, T., Zhang, P., and Wang, L.: Where the people are: Current trends and  
639 future potential targeted investments in urban trees for PM10 and temperature mitigation in 27 US cities.  
640 *Landscape and Urban Planning*, 177, 227-240, 2018.

641 Kordowski, K., and Kuttler, W.: Carbon dioxide fluxes over an urban park area. *Atmospheric Environment*, 44(23),  
642 2722-2730, 2010.

643 Kwon, H., Park, T. Y., Hong, J., Lim, J. H., and Kim, J.: Seasonality of Net Ecosystem Carbon Exchange in Two  
644 Major Plant Functional Types in Korea. *Asia-Pacific Journal of Atmospheric Sciences*, 45(2), 149-163, 2009.

645 Lee, K. Energy, water and CO<sub>2</sub> exchanges in an artificially constructed urban forest, Master Degree Dissertation,  
646 Yonsei University, Seoul, 2015.

647 Lee, K., Hong, J. W., Kim, J., and Hong, J.: Partitioning of net CO<sub>2</sub> exchanges at the city-atmosphere interface  
648 into biotic and abiotic components. *MethodsX*, 8, 101231, 2021.

649 Lietzke, B., Vogt, R., Feigenwinter, C., and Parlow, E.: On the controlling factors for the variability of carbon  
650 dioxide flux in a heterogeneous urban environment. *International Journal of climatology*, 35(13), 3921-3941, 2015.

651 Macdonald, R. W., Griffiths, R. F., and Hall, D. J.: An improved method for the estimation of surface roughness  
652 of obstacle arrays. *Atmospheric Environment*, 32(11), 1857-1864, 1998.

653 Mahecha, M. D., Reichstein, M., Carvalhais, N., Lasslop, G., Lange, H., Seneviratne, S. I., Vargas, R., Ammann,  
654 C., Arain, M. A., Cescatti, A., Janssens, I., Migliavacca, M., Montagnani, L., and Richardson, A.: Global  
655 convergence in the temperature sensitivity of respiration at ecosystem level. *Science*, 329(5993), 838-840, 2010.

656 McCarthy, M. P., Best, M. J., and Betts, R. A.: Climate change in cities due to global warming and urban effects.  
657 *Geophysical Research Letters*, 37(9), 2010.

658 Menzer, O., and McFadden, J. P.: Statistical partitioning of a three-year time series of direct urban net CO<sub>2</sub> flux  
659 measurements into biogenic and anthropogenic components. *Atmospheric Environment*, 170, 319-333, 2017.

660 Moriwaki, R., and Kanda, M.: Seasonal and diurnal fluxes of radiation, heat, water vapor, and carbon dioxide  
661 over a suburban area. *Journal of Applied Meteorology*, 43(11), 1700-1710, 2004.

662 Munger, J. W., Loescher, H. W., and Luo, H.: Measurement, tower, and site design considerations. In *Eddy  
663 Covariance* (pp. 21-58). Springer, Dordrecht, 2012.

664 Norton, B. A., Coutts, A. M., Livesley, S. J., Harris, R. J., Hunter, A. M., and Williams, N. S.: Planning for cooler  
665 cities: A framework to prioritise green infrastructure to mitigate high temperatures in urban landscapes. *Landscape  
666 and Urban Planning*, 134, 127-138, 2015.

667 Nowak, D. J.: Atmospheric carbon reduction by urban trees. *Journal of Environmental Management*, 37(3), 207-  
668 217, 1993.

669 Nowak, D. J., Crane, D. E., Stevens, J. C., Hoehn, R. E., Walton, J. T., and Bond, J.: A ground-based method of  
670 assessing urban forest structure and ecosystem services. *Arboriculture and Urban Forestry*. 34 (6): 347-358., 34(6),  
671 2008.

672 Oke, T. R.: The energetic basis of the urban heat island. *Quarterly Journal of the Royal Meteorological Society*,  
673 108(455), 1-24, 1982.

674 Oke, T. R.: The micrometeorology of the urban forest. *Philosophical Transactions of the Royal Society of London.  
675 B, Biological Sciences*, 324(1223), 335-349, 1989.

676 Oke, T. R., Johnson, G. T., Steyn, D. G., and Watson, I. D.: Simulation of surface urban heat islands under 'ideal'  
677 conditions at night part 2: Diagnosis of causation. *Boundary-Layer Meteorology*, 56(4), 339-358, 1991.

678 Oke, T.R., Mills, G., Christen, A., Voogt, J.A.: *Urban Climates*. Cambridge University Press, U.K., 2017.

679 Pastorello, G., Trotta, C., Canfora, E., Chu, H., Christianson, D., Cheah, Y. W., Poindexter, C., Chen,  
680 J., Elbashandy, A., Humphrey, M., Isaac, P., Polidori, D., Ribeca, A., van Ingen, C., Zhang, L., Amiro,

681 B., Ammann, C., Arain, M.A., Ardö, J., Arkebauer, T., Arndt, S.K., Arriga, N., Aubinet, M., Aurela,  
682 M., Baldocchi, D., Barr, A., Beamesderfer, E., Marchesini, L.B., Bergeron, O., Beringer, J., Bernhofer,  
683 C., Berveiller, D., Billesbach, D., Black, T.A., Blanken, P.D., Bohrer, G., Boike, J., Bolstad, P.V., Bonal,  
684 D., Bonnefond, J.-M., Bowling, D.R., Bracho, R., Brodeur, J., Brümmer, C., Buchmann, N., Burban, B., Burns,  
685 S.P., Buysse, P., Cale, P., Cavagna, M., Cellier, P., Chen, S., Chini, I. Christensen, T.R., Cleverly, J., Collalti,  
686 A., Consalvo, C., Cook, B.D., Cook, D., Coursolle, C., Cremonese, E., Curtis, P.S., D'Andrea, E., da Rocha,  
687 H., Dai, X., Davis, K.J., De Cinti, B., de Grandcourt, A., De Ligne, A., De Oliveira, R.C., Delpierre, N., Desai,  
688 A.R., Di Bella, C.M., di Tommasi, P., Dolman, H., Domingo, F., Dong, G., Dore, S., Duce, P., Dufrêne, E., Dunn,  
689 A., Dušek, J., Eamus, D., Eichelmann, U., ElKhidir, H.A.M., Eugster, W., Ewenz, C.M., Ewers, B., Famulari,  
690 D., Fares, S., Feigenwinter, I., Feitz, A., Fensholt, R., Filippa, G., Fischer, M., Frank, J., Galvagno, M., Gharun,  
691 M., Gianelle, D., Gielen, B., Gioli, B., Gitelson, A., Goded, I., Goeckede, M., Goldstein, A.H., Gough,  
692 C.M., Goulden, M.L., Graf, A., Griebel, A., Gruening, C., Grünwald, T., Hammerle, A., Han, S., Han,  
693 X., Hansen, B.U., Hanson, C., Hatakka, J., He, Y., Hehn, M., Heinesch, B., Hinko-Najera, N., Hörtnagl,  
694 L., Hutley, L., Ibrom, A., Ikawa, H., Jackowicz-Korczynski, M., Janouš, D., Jans, W., Jassal, R., Jiang, S., Kato,  
695 T., Khomik, M., Klatt, J., Knohl, A., Knox, S., Kobayashi, H., Koerber, G., Kolle, O., Kosugi, Y., Kotani,  
696 A., Kowalski, A., Kruijt, B., Kurbatova, J., Kutsch, W.L., Kwon, H., Launiainen, S., Laurila, T., Law,  
697 B., Leuning, R., Li, Y., Liddell, M., Limousin, J.-M., Lion, M., Liska, A.J., Lohila, A., López-Ballesteros,  
698 A., López-Blanco, E., Loubet, B., Loustau, D., Lucas-Moffat, A., Lüers, J., Ma, S., Macfarlane, C., Magliulo,  
699 V., Maier, R., Mammarella, I., Manca, G., Marcolla, B., Margolis, H.A., Marras, S., Massman, W., Mastepanov,  
700 M., Matamala, R., Matthes, J.H., Mazzenga, F., McCaughey, H., McHugh, I., McMillan, A.M.S., Merbold,  
701 L., Meyer, W., Meyers, T., Miller, S.D., Minerbi, S., Moderow, U., Monson, R.K., Montagnani, L., Moore,  
702 C.E., Moors, E., Moreaux, V., Moureaux, C., Munger, J.W., Nakai, T., Neiryneck, J., Nesic, Z., Nicolini,  
703 G., Noormets, A., Northwood, M., Noretto, M., Nouvellon, Y., Novick, K., Oechel, W., Olesen, J.E., Ourcival,  
704 J.-M., Papuga, S.A., Parmentier, F.-J., Paul-Limoges, E., Pavelka, M., Peichl, M., Pendall, E., Phillips,  
705 R.P., Pilegaard, K., Pirk, N., Posse, G., Powell, T., Prasse, H., Prober, S.M., Rambal, S., Rannik, Ü., Raz-Yaseef,  
706 N., Reed, D., de Dios, V.R., Restrepo-Coupe, N., Reverter, B.R., Roland, M., Sabbatini, S., Sachs, T., Saleska,  
707 S.R., Sánchez-Cañete, E.P., Sanchez-Mejia, Z.M., Schmid, H.P., Schmidt, M., Schneider, K., Schrader,  
708 F., Schroder, I., Scott, R.L., Sedlák, P., Serrano-Ortíz, P., Shao, C., Shi, P., Shironya, I., Siebicke, L., Šigut,  
709 L., Silberstein, R., Sirca, C., Spano, D., Steinbrecher, R., Stevens, R.M., Sturtevant, C., Suyker, A., Tagesson,  
710 T., Takanashi, S., Tang, Y., Tapper, N., Thom, J., Tiedemann, F., Tomassucci, M., Tuovinen, J.-P., Urbanski,  
711 S., Valentini, R., van der Molen, M., van Gorsel, E., van Huissteden, K., Varlagin, A., Verfaillie, J., Vesala,  
712 T., Vincke, C., Vitale, D., Vygodskaya, N., Walker, J.P., Walter-Shea, E., Wang, H., Weber, R., Westermann,  
713 S., Wille, C., Wofsy, S., Wohlfahrt, G., Wolf, S., Woodgate, W., Li, Y., Zampedri, R., Zhang, J., Zhou, G., Zona,  
714 D., Agarwal, D., Biraud, S., Torn, M., and Papale, D.: The FLUXNET2015 dataset and the ONEFlux processing  
715 pipeline for eddy covariance data. *Scientific Data*, 7(1), 1-27, 2020.

716 Pataki, D. E., Bowling, D. R., and Ehleringer, J. R.: Seasonal cycle of carbon dioxide and its isotopic composition  
717 in an urban atmosphere: Anthropogenic and biogenic effects. *Journal of Geophysical Research: Atmospheres*, 108,  
718 D23, <https://doi.org/10.1029/2003JD003865>, 2003.

719 Peters, E. B., and McFadden, J. P.: Continuous measurements of net CO<sub>2</sub> exchange by vegetation and soils in a  
720 suburban landscape. *Journal of Geophysical Research: Biogeosciences*, 117, G3,  
721 <https://doi.org/10.1029/2011JG001933>, 2012.

722 Piao, S., Luysaert, S., Ciais, P., Janssens, I. A., Chen, A., Cao, C., Fang, J., Friedlingstein, P., Luo, Y., and Wang,  
723 S.: Forest annual carbon cost: A global-scale analysis of autotrophic respiration. *Ecology*, 91(3), 652-661, 2010.

724 Rahmstorf, S., and Coumou, D.: Increase of extreme events in a warming world. *Proceedings of the National  
725 Academy of Sciences*, 108(44), 17905-17909, 2011.

726 Randerson, J.T., Chapin III, F.S., Harden, J.W., Neff, J.C. and Harmon, M.E.: Net ecosystem production: a  
727 comprehensive measure of net carbon accumulation by ecosystems. *Ecological Applications*, 12(4), 937-947,  
728 2002.

729 Raupach, M. R., Antonia, R. A., and Rajagopalan, S.: Rough-wall turbulent boundary layers, *Applied Mechanics  
730 Reviews*, 44(1), 1-25, 1991.

731 Rowntree, R. A., and Nowak, D. J.: Quantifying the role of urban forests in removing atmospheric carbon dioxide.  
732 *Journal of Arboriculture*. 17 (10): 269-275., 17(10), 1991.

733 Roy, S., Byrne, J., and Pickering, C.: A systematic quantitative review of urban tree benefits, costs, and assessment  
734 methods across cities in different climatic zones. *Urban Forestry and Urban Greening*, 11(4), 351-363, 2012.

735 Schmid, H. P., Grimmond, C. S. B., Cropley, F., Offerle, B., and Su, H. B.: Measurements of CO<sub>2</sub> and energy  
736 fluxes over a mixed hardwood forest in the mid-western United States. *Agricultural and Forest Meteorology*,  
737 103(4), 357-374, 2000.

738 Schmid, H. P., Su, H. B., Vogel, C. S., and Curtis, P. S.: Ecosystem-atmosphere exchange of carbon dioxide over  
739 a mixed hardwood forest in northern lower Michigan. *Journal of Geophysical Research: Atmospheres*, 108(D14),  
740 2003.

741 Shashua-Bar, L., and Hoffman, M. E.: Vegetation as a climatic component in the design of an urban street: An  
742 empirical model for predicting the cooling effect of urban green areas with trees. *Energy and Buildings*, 31(3),  
743 221-235, 2000.

744 Shim, C., J. Hong, J. Hong, Y. Kim, M. Kang, B. Thakuri, Y. Kim, J. Chun: Evaluation of MODIS GPP over a  
745 complex ecosystem in East Asia: A case of Gwangneung flux tower in Korea, *Advances in Space Research*, 54,  
746 2296-2308, 2014.

747 Spronken-Smith, R. A., Oke, T. R., and Lowry, W. P.: Advection and the surface energy balance across an  
748 irrigated urban park. *International Journal of Climatology: A Journal of the Royal Meteorological Society*, 20(9),  
749 1033-1047. 2000.

750 Stagakis, S., Chrysoulakis, N., Spyridakis, N., Feigenwinter, C., and Vogt, R.: Eddy Covariance measurements  
751 and source partitioning of CO<sub>2</sub> emissions in an urban environment: Application for Heraklion, Greece.  
752 *Atmospheric Environment*, 201, 278-292, 2019.

753 Stewart, I. D.: A systematic review and scientific critique of methodology in modern urban heat island literature.  
754 *International Journal of Climatology*, 31(2), 200-217, 2011.

755 Stewart, I. D., and Oke, T. R.: Local climate zones for urban temperature studies. *Bulletin of the American  
756 Meteorological Society*, 93(12), 1879-1900, 2012.



757 Stoy, P. C., Katul, G. G., Siqueira, M. B., Juang, J. Y., Novick, K. A., Uebelherr, J. M., and Oren, R.: An evaluation  
758 of models for partitioning eddy covariance-measured net ecosystem exchange into photosynthesis and respiration.  
759 *Agricultural and Forest Meteorology*, 141(1), 2-18, 2006.

760 Suyker, A.E. and Verma, S.B.: Interannual water vapor and energy exchange in an irrigated maize-based  
761 agroecosystem. *Agricultural and Forest Meteorology*, 148, 417-427, 2008.

762 Takanashi, S., Kosugi, Y., Tanaka, Y., Yano, M., Katayama, T., Tanaka, H., and Tani, M.. CO<sub>2</sub> exchange in a  
763 temperate Japanese cypress forest compared with that in a cool-temperate deciduous broad-leaved forest.  
764 *Ecological Research*, 20(3), 313-324, 2005.

765 Ueyama, M., and Ando, T.: Diurnal, weekly, seasonal, and spatial variabilities in carbon dioxide flux in different  
766 urban landscapes in Sakai, Japan. *Atmospheric Chemistry and Physics*, 16(22), 14727-14740, 2016.

767 United Nations, Department of Economic and Social Affairs, Population Division: World Urbanization Prospects:  
768 The 2018 Revision (ST/ESA/SER.A/420). New York: United Nations, 2019.

769 Velasco, E., and Roth, M.: Cities as net sources of CO<sub>2</sub>: Review of atmospheric CO<sub>2</sub> exchange in urban  
770 environments measured by eddy covariance technique. *Geography Compass*, 4(9), 1238-1259, 2010.

771 Velasco, E., Roth, M., Tan, S. H., Quak, M., Nabarro, S. D. A., and Norford, L.: The role of vegetation in the  
772 CO<sub>2</sub> flux from a tropical urban neighbourhood, *Atmospheric Chemistry and Physics*, 13, 10185–10202,  
773 <https://doi.org/10.5194/acp-13-10185-2013>, 2013.

774 Velasco, E., Roth, M., Norford, L., and Molina, L. T.: Does urban vegetation enhance carbon sequestration?,  
775 *Landscape and Urban Planning*, 148, 99-107, 2016.

776 Wang, L., Lee, X., Schultz, N., Chen, S., Wei, Z., Fu, C., Gao, Y., Yang, Y, and Lin, G.: Response of surface  
777 temperature to afforestation in the Kubuqi Desert, Inner Mongolia. *Journal of Geophysical Research:*  
778 *Atmospheres*, 123, 948-964, 2018.

779 Ward, H. C., Evans, J. G., and Grimmond, C. S. B.: Multi-season eddy covariance observations of energy, water  
780 and carbon fluxes over a suburban area in Swindon, UK. *Atmospheric Chemistry and Physics*, 13(9), 4645-4666,  
781 2013.

782 Ward, H. C., Kotthaus, S., Grimmond, C. S. B., Bjarkegren, A., Wilkinson, M., Morrison, W. T. J., Evans, J. G.,  
783 Morrison, J. I. L. m and Iamarino, M.: Effects of urban density on carbon dioxide exchanges: Observations of dense  
784 urban, suburban and woodland areas of southern England. *Environmental Pollution*, 198, 186-200, 2015.

785 Weissert, L. F., Salmund, J. A., and Schwendenmann, L.: A review of the current progress in quantifying the  
786 potential of urban forests to mitigate urban CO<sub>2</sub> emissions. *Urban Climate*, 8, 100-125, 2014.

787 York D., Evensen N., Martinez M., and Delgado J.: Unified equations for the slope, intercept, and standard errors  
788 of the best straight line. *American Journal of Physics*, 72(3), 367-375, 2004.

789 Yu, C., and Hien, W. N.: Thermal benefits of city parks. *Energy and Buildings*, 38(2), 105-120, 2006.

790

791

792 Table 1. Details of the stations used in this study.

Sites	Location	Local climate zone	Measurement height (m)
Eddy covariance station			
SFP (Seoul Forest Park)	37.5446°N, 127.0379°E	Dense tree (LCZ <sub>A</sub> )	12.2
EP (Eunpyeong)	37.6350°N, 126.9287°E	Compact highrise (LCZ <sub>1</sub> )	30
Weather station			
SD (Seongdong)	37.5472°N, 127.0389°E	Open midrise and scatted trees (LCZ <sub>5B</sub> )	25
CBD			
(Gangnam)	37.5134°N, 127.0467°E	Compact midrise and highrise (LCZ <sub>21</sub> )	20
(Seocho)	37.4889°N, 127.0156°E	Compact highrise and open midrise (LCZ <sub>15</sub> )	13
(Songpa)	37.5115°N, 127.0967°E		43
GP (Gimpo)	37.5722°N, 126.7751°E	Low plants (LCZ <sub>D</sub> )	1.5

793

794

795 Table 2. Daytime Bowen ratio ( $\beta = Q_H/Q_E$ ) in summer at the SFP and other urban sites of the similar vegetation  
 796 cover fraction ( $\lambda_v$ ).

Site name	$\beta$	$\lambda_v$	References
SFP	0.56	0.57	this study
Basel-Sperrstrasse	2.5	0.16	Christen and Vogt (2004)
Basel-Spaleiring	2.3	0.32	Christen and Vogt (2004)
Tucson	1.8	0.42	Grimmond and Oke (1995)
Sacramento	1.4	0.42	Grimmond and Oke (1995)
Chicago	0.8	0.44	Grimmond and Oke (1995)
Los Angeles	1.4	0.41	Grimmond and Oke (1995)
Kansas City	0.48	0.58	Balogun et al. (2009)
Oberhausen-suburban	0.36	0.69	Goldbach and Kuttler (2013)

797

798

799 Table 3. Gap-filled annual budgets for surface energy fluxes and precipitation (P).

	$ET$ (mm)	$Q_H$ (MJ m <sup>-2</sup> )	$Q_E$ (MJ m <sup>-2</sup> )	$Q^*$ (MJ m <sup>-2</sup> )	P (mm)
1 <sup>st</sup> year (2013.06 – 2014.05)	367	726	896	1797	1256
2 <sup>nd</sup> year (2014.06 – 2015.05)	320	867	781	1848	932
Mean annual sum of two-year	344	797	839	1823	1094

800

801

802 Table 4. Gap-filled annual budgets for  $F_C$  (observed by EC measurement) and its components, indicating  
 803 ecosystem respiration ( $RE$ ), photosynthetic uptake by vegetation ( $GPP$ ), vehicle emissions ( $E_R$ ), and building  
 804 emissions ( $E_B$ ). All fluxes are in  $\text{kg CO}_2 \text{ m}^{-2} \text{ year}^{-1}$ .

Sites	$F_C$	$RE$	$GPP$	$E_R$	$E_B$
1 <sup>st</sup> (2013.06 – 2014.05) year	6.6	5.1 (77%)	4.7 (70%)	5.4 (81%)	1.0 (15%)
2 <sup>nd</sup> (2014.06 – 2015.05) year	7.6	5.0 (65%)	4.5 (59%)	5.4 (71%)	1.9 (25%)
Mean annual sum of two-year	7.1	5.1 (71%)	4.6 (64%)	5.4 (76%)	1.5 (20%)

805

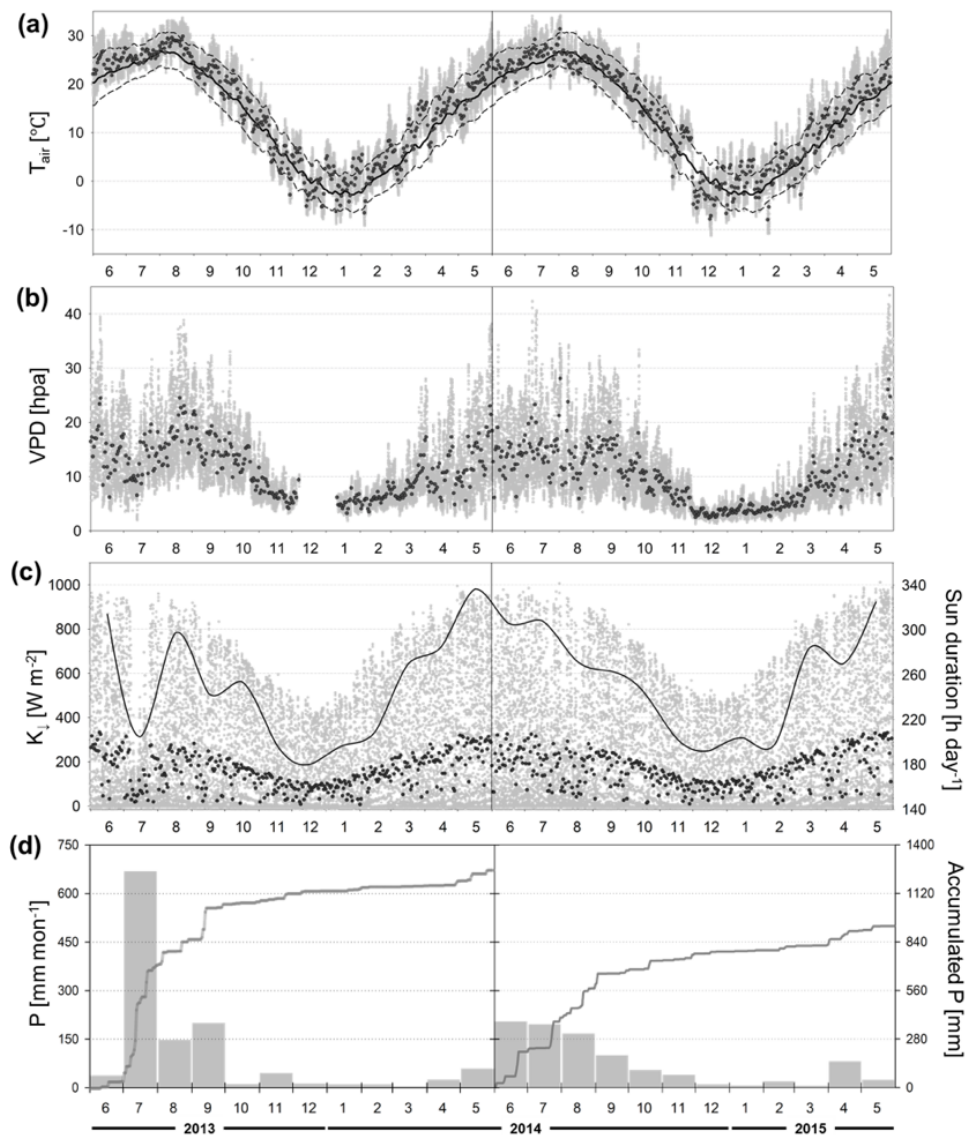
806

807 Table 5. Annual budgets of biogenic  $F_C$  components and ratios in deciduous broadleaf forests in similar climatic  
 808 conditions reported in previous studies. All fluxes are in  $\text{kg CO}_2 \text{ m}^{-2} \text{ year}^{-1}$ .

Site name	Reference	MAT (°C)	MAP (mm)	maximum LAI	<i>RE</i>	<i>GPP</i>	<i>NBE</i>	<i>RE/GPP</i>
Seoul Forest Park	This study	13.9	1094	1.6	5.1	4.6	+0.5	1.11
Nagoya urban forest	Awal et al. (2010)	15.9	1680	5.5	4.9	6.2	-1.3	0.74
Toyota rural forest		14.5	1518	4.5	2.6	4.6	-2.0	0.56
Gwangneung deciduous forest	Kwon et al. (2010)	12.8	1487	5	3.8	4.1	-0.3	0.93
Kiryu Experimental Watershed	Takanashi et al. (2005)	14.1	1309	5.5	3.9	5.6	-1.7	0.70
FLUXNET2015 dataset*	Pastorello et al. (2020)	14.5	1113		4.1	6.0	-1.9	0.68

809 \*Average value of 8-year data from 4 sites having mean annual temperature (MAT) of 12-16°C, mean annual  
 810 precipitation (MAP) of 900-2000 mm.

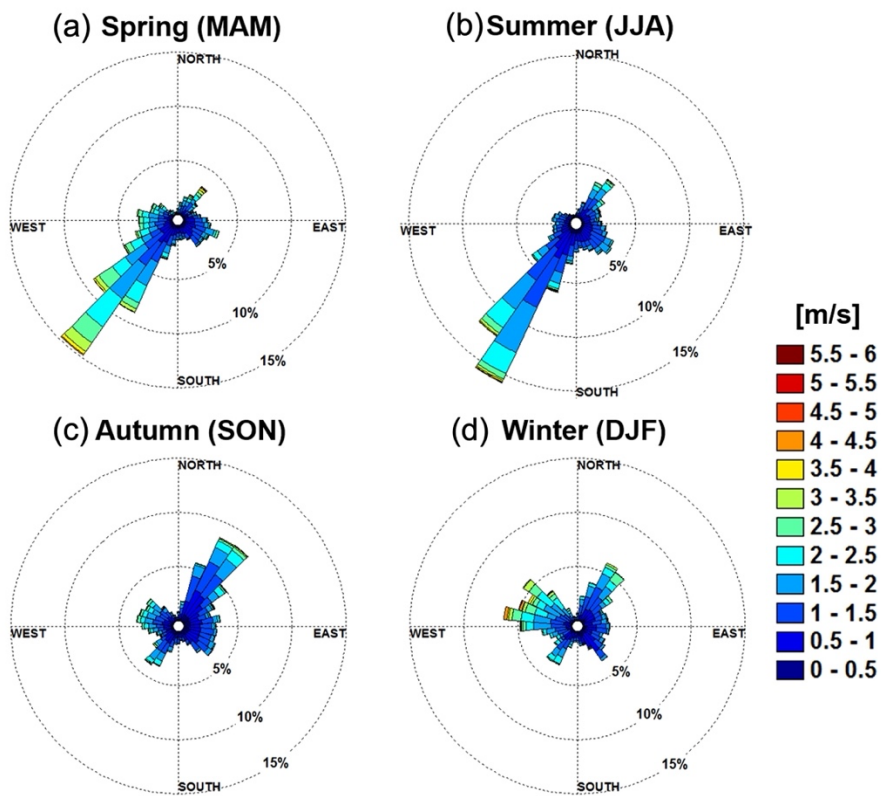
811



812

813 Figure 1. Climatic conditions of the SFP for two years from June 2013 to May 2015: 30-min (gray dots) and daily  
 814 mean (black dots) (a) air temperature with 30-year normal values of Seoul (daily mean; solid line, min and max;  
 815 dashed lines), (b) vapor pressure deficit (VPD) and missing data existing on December 2013, (c) downward  
 816 shortwave radiation ( $K_{\downarrow}$ ) and monthly averaged sunshine duration per day (black line), (d) monthly precipitation  
 817 (gray bars) and yearly accumulated precipitation (solid line).

818



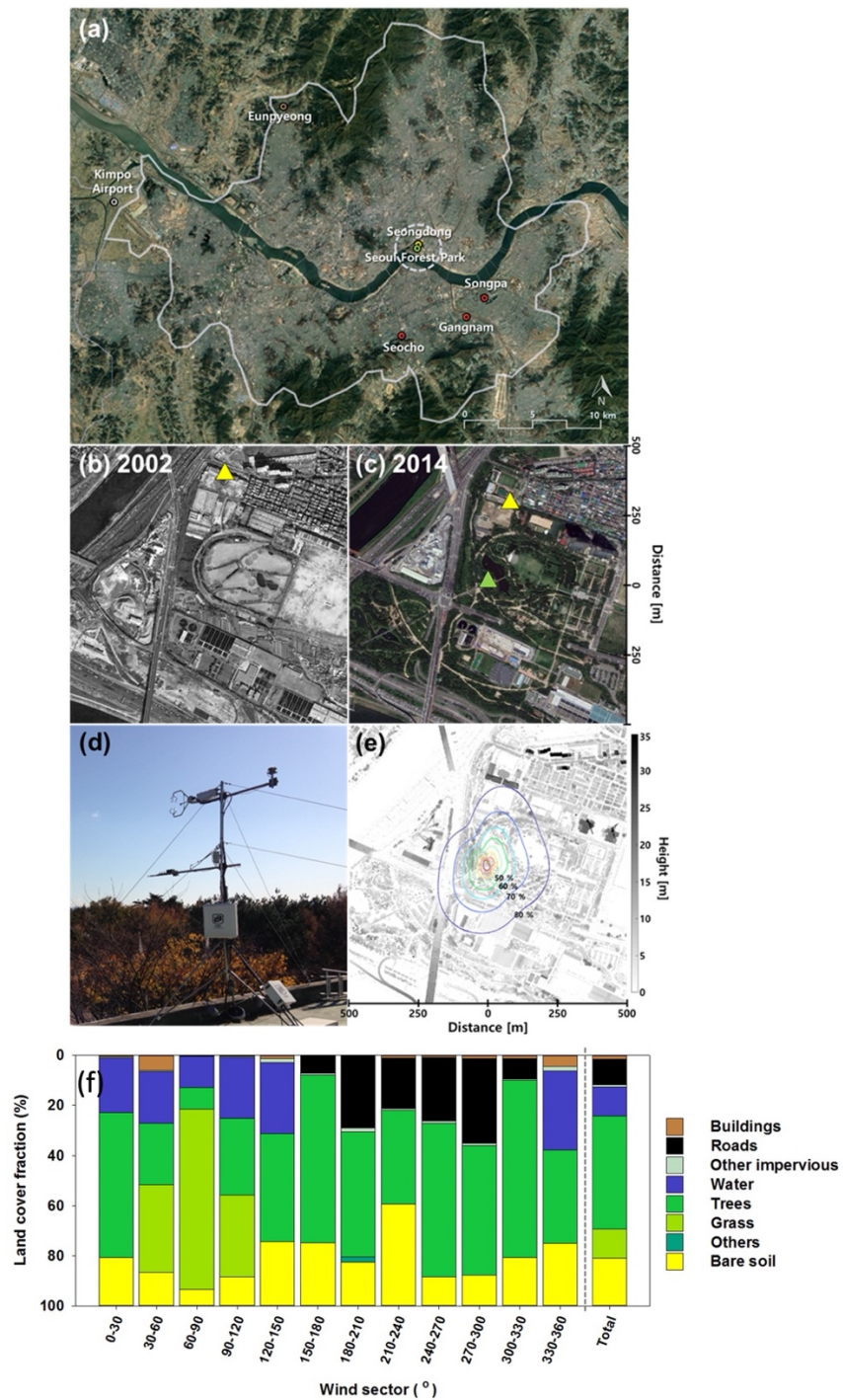
819

820

821 Figure 2. Wind roses with seasons: (a) spring (b) summer (c) autumn (d) winter.

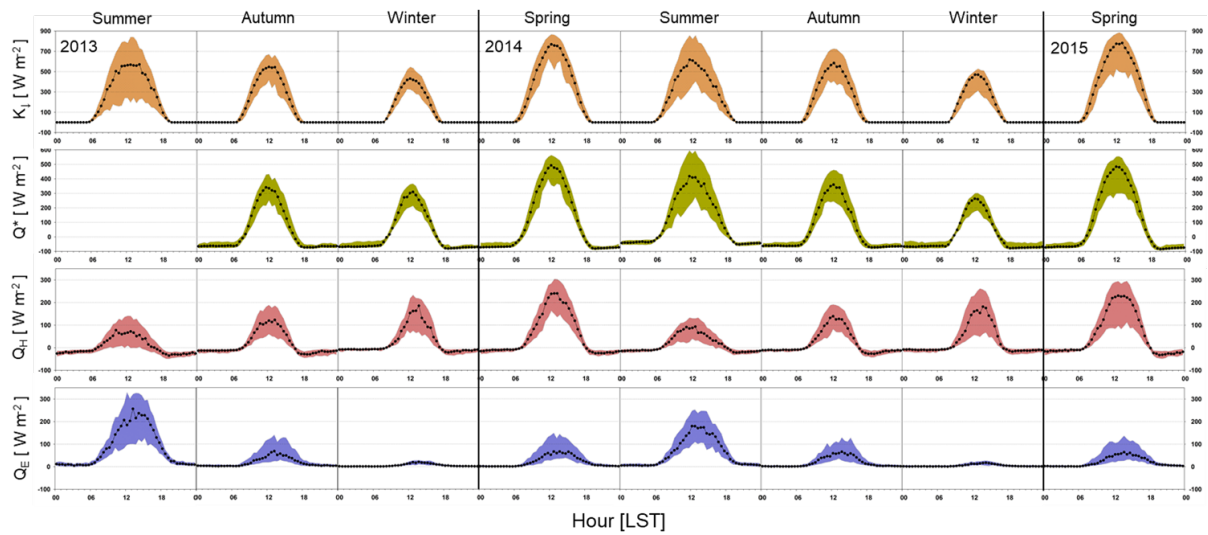
822





824

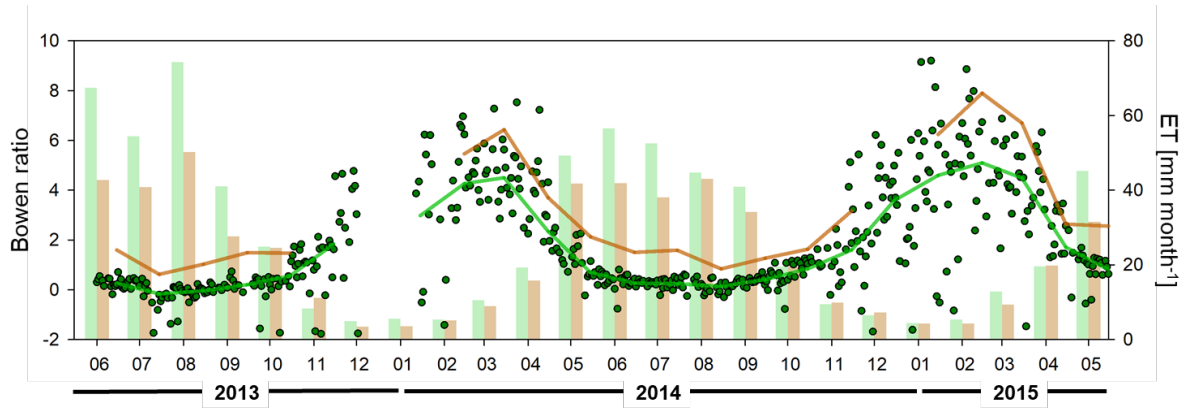
825 Figure 3. Site descriptions. (a) Location of the stations in Seoul (modified from map data © Google Earth 2019),  
 826 (b) aerial photographs around Seoul Forest Park (SFP) in 2002 before the creation of the park and (c) in 2014  
 827 during the observation period (SFP; *green triangle*, SD; *yellow triangle*), (d) photograph of the SFP station, (e)  
 828 footprint climatology (Hsieh et al., 2000) with the height of surrounding obstacles around the SFP station, and (f)  
 829 land cover fraction within a 150 m radius around a flux tower.



830

831 Figure 4. Diurnal variations of surface energy fluxes. Seasonal median diurnal variations (*points*) and interquartile  
 832 ranges (*shaded*) of 30-min downward shortwave radiation ( $K_l$ ), net radiation ( $Q^*$ ), sensible heat flux ( $Q_H$ ), and  
 833 latent heat flux ( $Q_E$ ) for two years. Since the net radiation system was installed in September 2013, there was no  
 834  $Q^*$  value in the first summer.

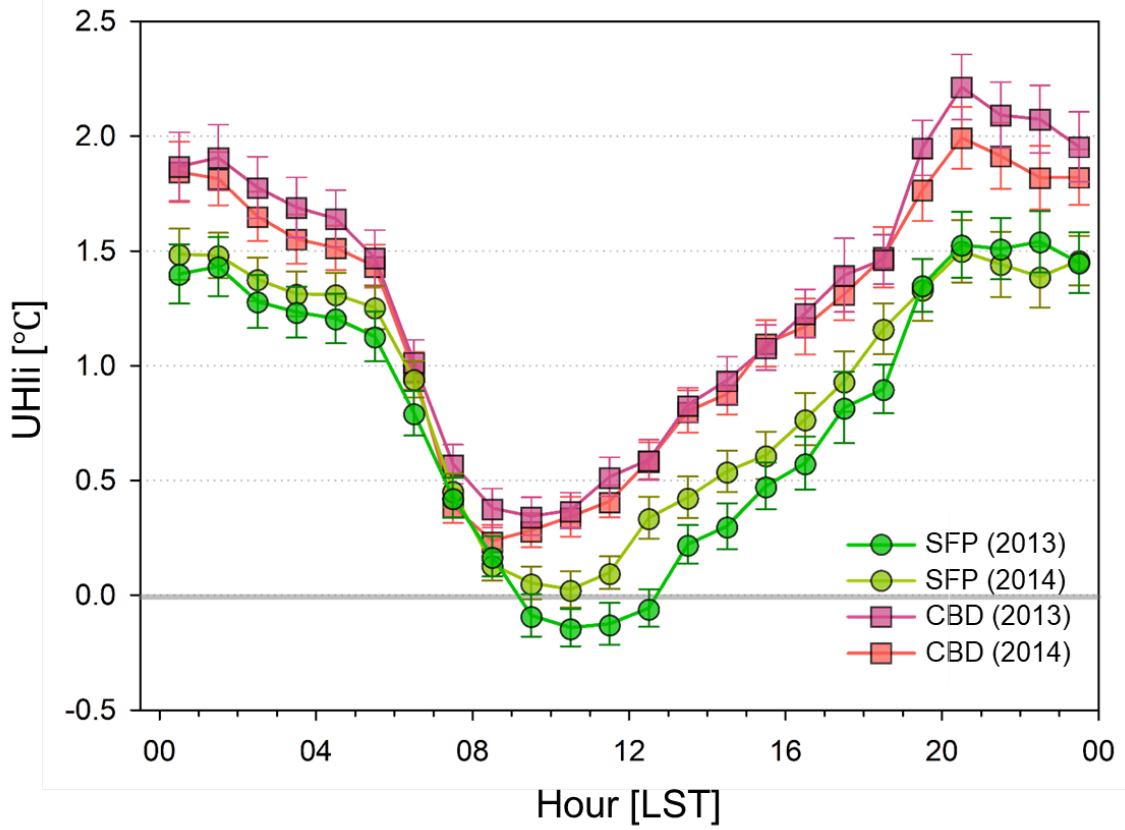
835



836

837 Figure 5. Daily Bowen ratio ( $\beta = \sum Q_H / \sum Q_E$ ; dots), monthly Bowen ratio (lines), and gap-filled monthly  
 838 evapotranspiration (ET; bars) for two years (SFP; green, EP; brown).

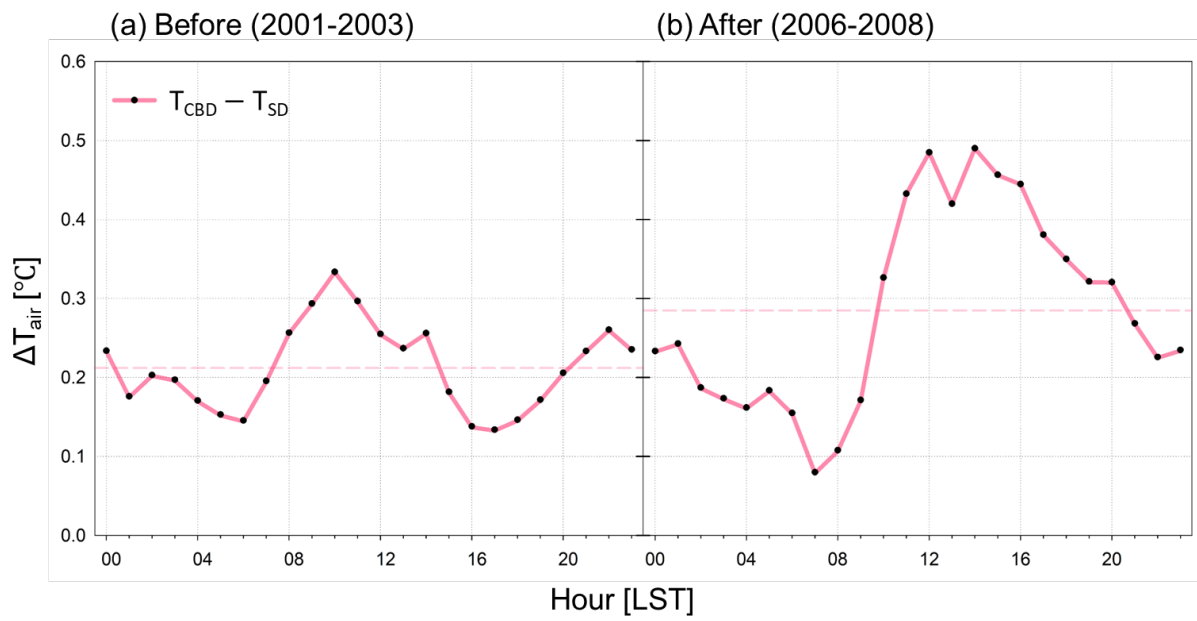
839



840

841 Figure 6. Hourly mean diurnal variation of the urban heat island intensity (UHIi) of the SFP and CBD in the  
 842 summer of 2013 and 2014. The error bars represent standard errors.

843



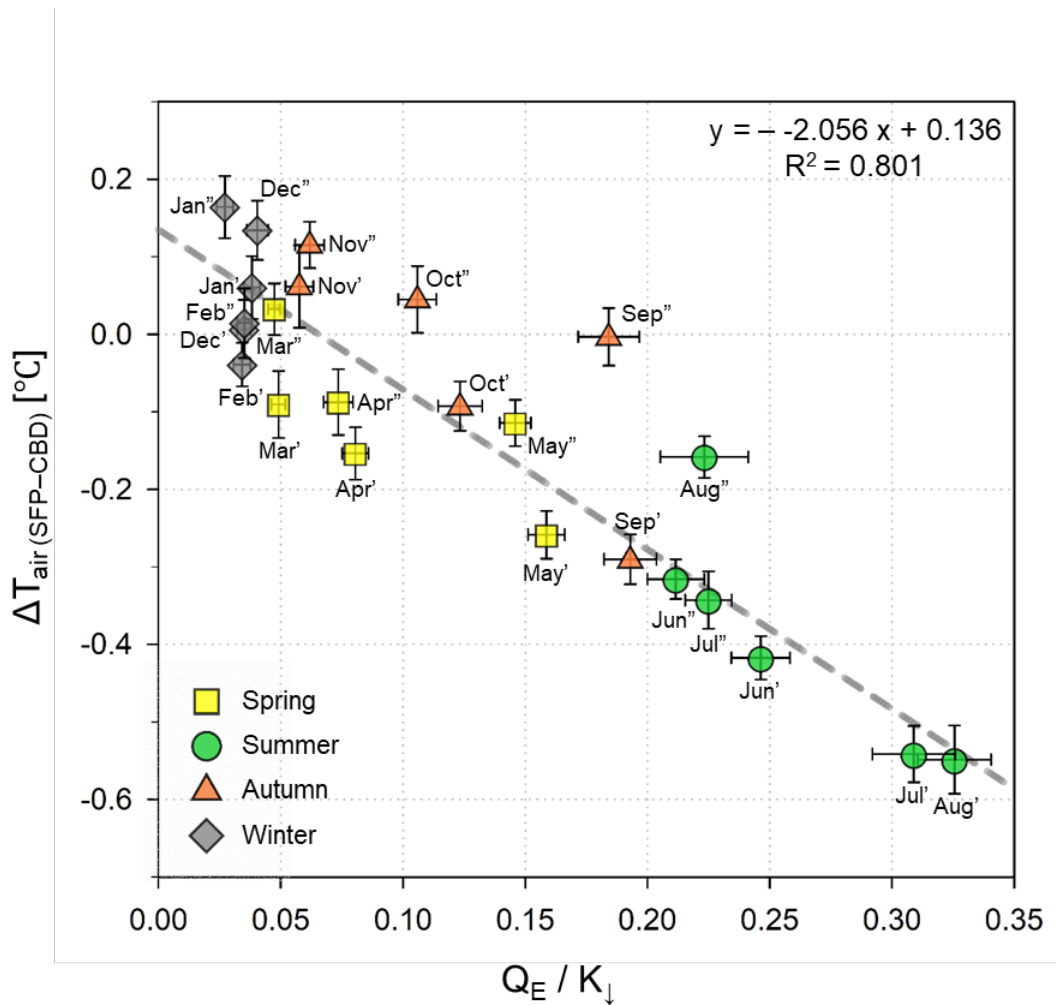
844

845 Figure 7. Mean diurnal pattern of air temperature difference ( $\Delta T_{air}$ ) between CBD and SD in summer (a) before

846 and (b) after the construction of the park. CBD indicates an average of three automatic weather stations (Gangnam,

847 Seocho, Songpa) in Seoul. The red dash line indicates the mean  $\Delta T_{air}$  before and after the construction of the park

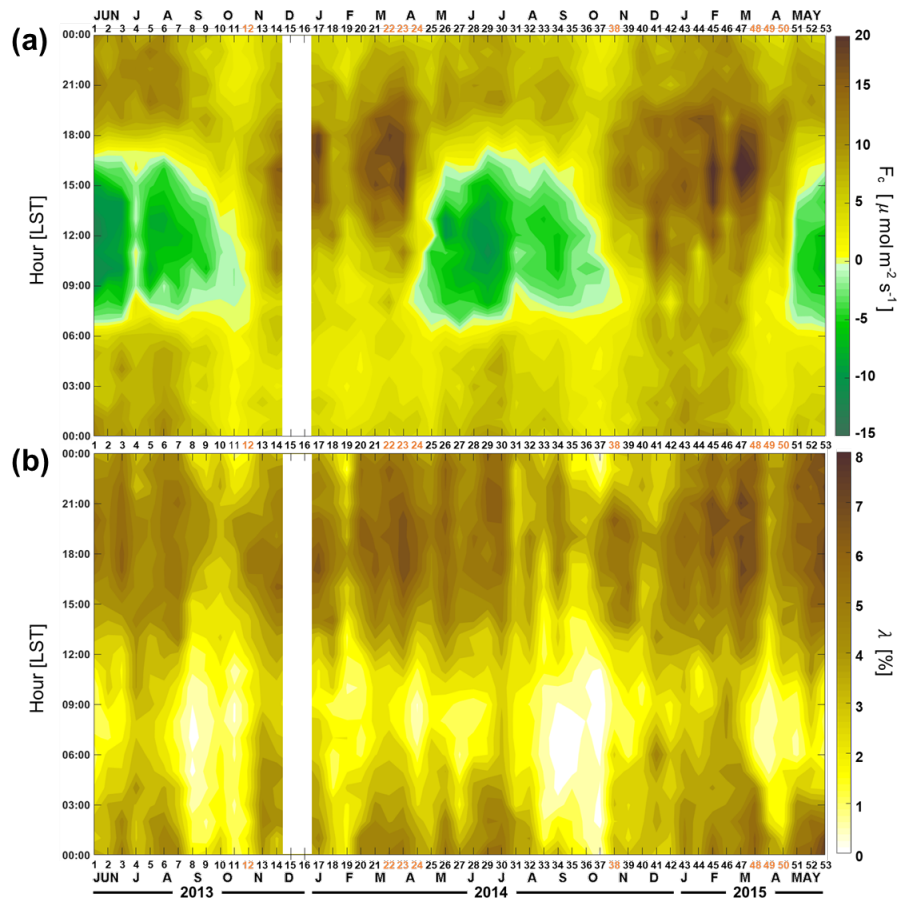
848  
849



850

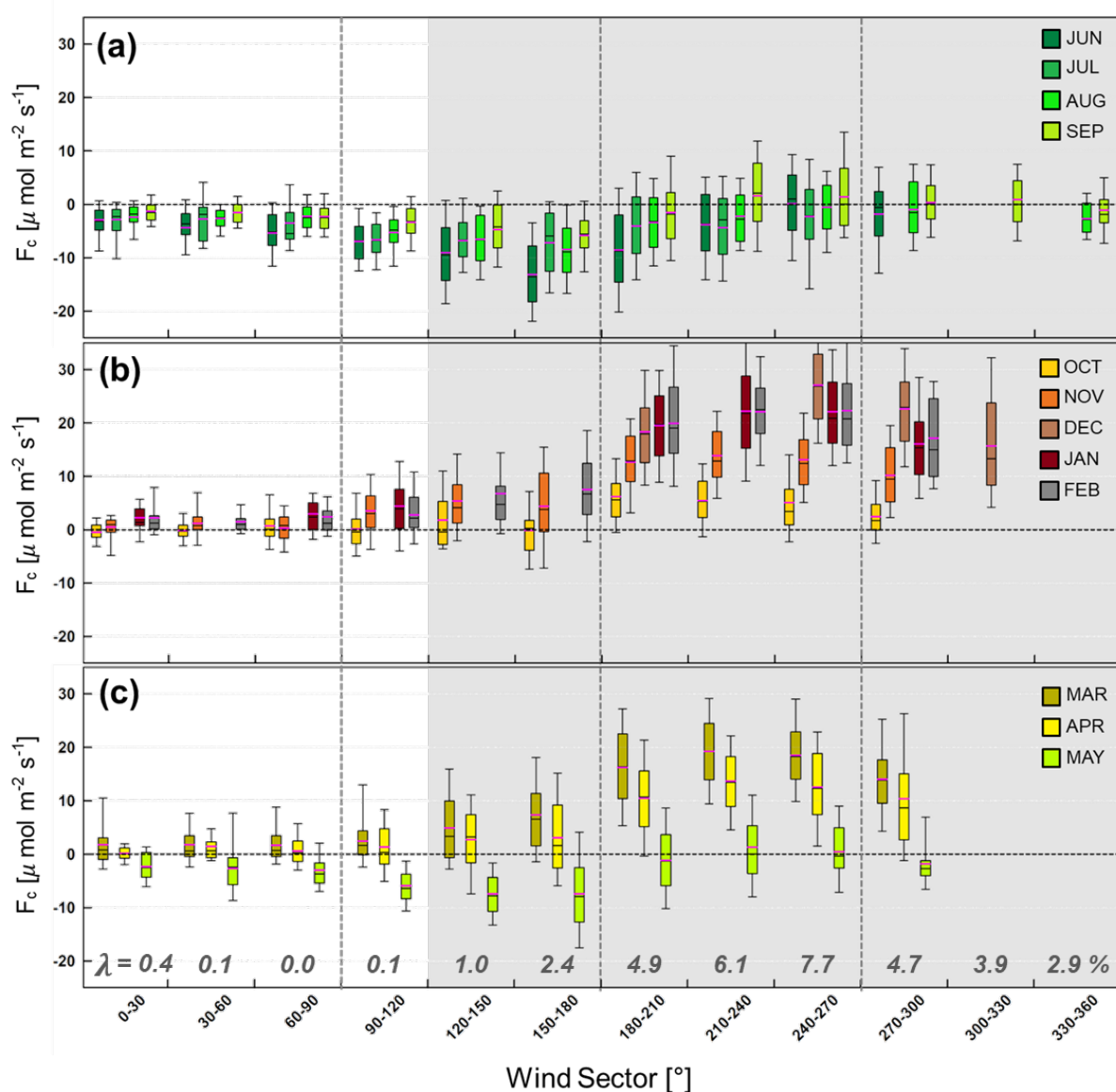
851 Figure 8. Relationship between the ratio of monthly  $Q_E$  to  $K_d$  and mean air temperature difference between SFP  
852 and CBD during the daytime ( $K_d > 120 \text{ W m}^{-2}$ ) for two years. The quotation and double-quotation marks on the  
853 scatter indicate the first and second year of the observation period, respectively. The error bars represent standard  
854 errors based on daily values, and the grey dotted line is calculated using linear regression model considering errors  
855 in both axes (York et al., 2004).

856



858

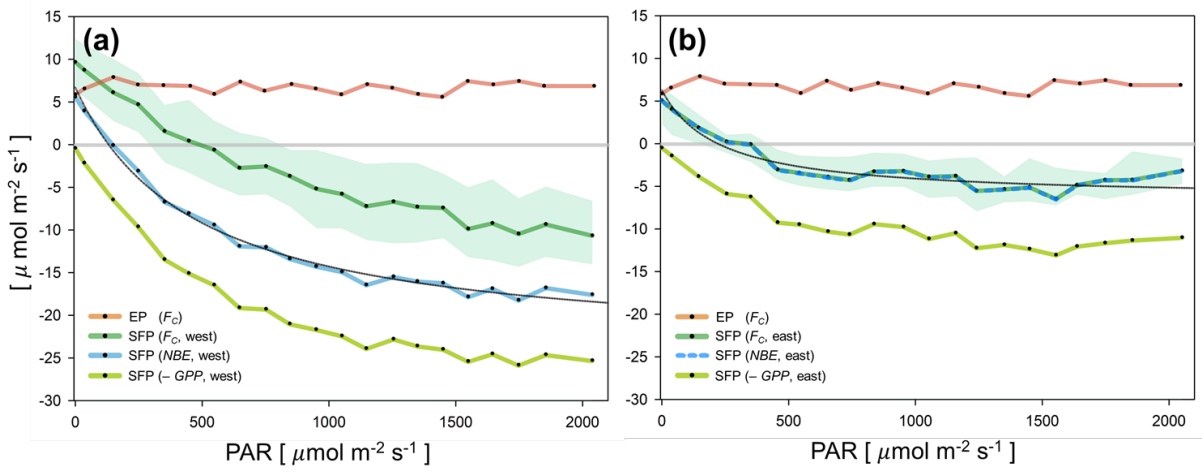
859 Figure 9. (a) Temporal variation of hourly averaged  $F_c$  and (b) footprint-weighted road fraction ( $\lambda$ ) as every two-  
 860 week average (x-axis: the date, y-axis: time of day). In December 2013, there was a gap for approximately 4  
 861 weeks due to the power system failure. The yellow numbers in x-axis indicate the transition period when traffic  
 862 emissions ( $E_R$ ) contributes to the observed  $F_c$  significantly.



863

864 Figure 10. Monthly boxplots of daytime ( $K_1 > 120 \text{ W m}^{-2}$ )  $F_c$  by wind direction. Boxes have a minimum of 882  
 865 samples. Box limits are upper and lower quartiles, and whiskers are distances of 1.5 times the interquartile range  
 866 from each quartile. Median and mean values are indicated by the black and pink horizontal lines. The average  
 867 source area weighted road fractions ( $\lambda$ ) are shown below the graph, and wind sectors with  $\lambda$  greater than 1% are  
 868 shaded in gray.





870 Figure 11. During the growing season (June–August 2013, 2014) when  $E_B$  is negligible, light-response curves as a function of photosynthetically active radiation (PAR, in bins of  $100 \mu\text{mol m}^{-2} \text{s}^{-1}$ ): (a) for the western sectors ( $150^\circ < \Phi < 300^\circ$ ) and (b) for the eastern sectors ( $30^\circ < \Phi < 90^\circ$ ). Black line is a rectangular hyperbolic equation fitting net biome exchange ( $NBE = RE - GPP = F_C - E_R$ ) to PAR, and EP (brown line) is a light-response curve for the high-rise high-population residential area in Seoul. The shaded areas indicate interquartile range.

875

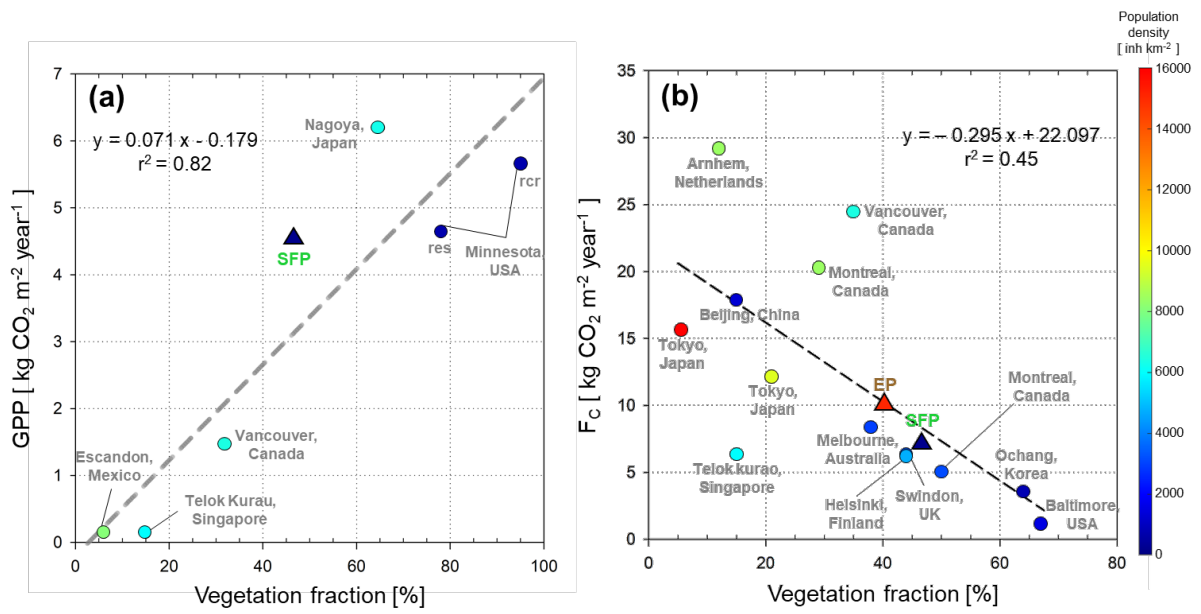
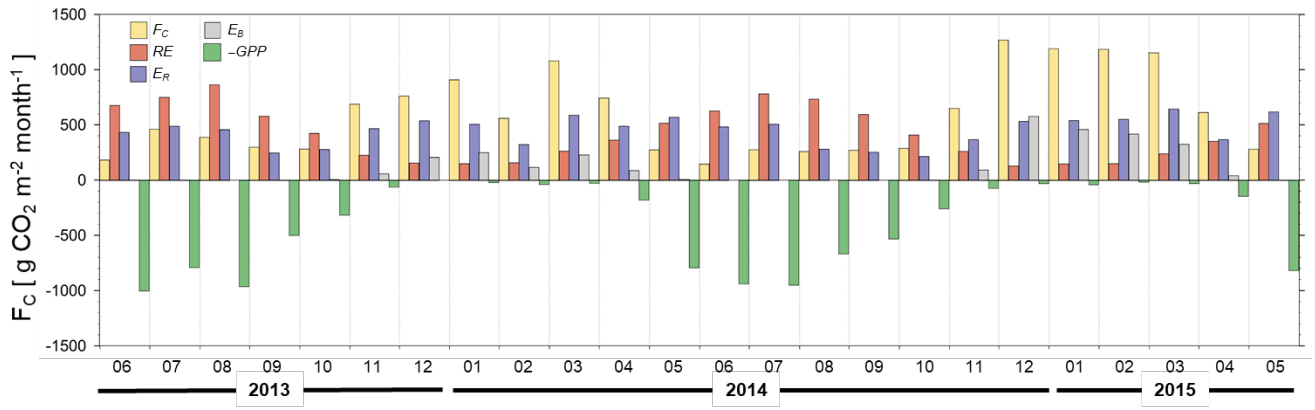


Figure 12. Relationship between vegetation fraction (a) annual *GPP* and (b) annual *F<sub>c</sub>* in urban sites. Dashed line in (a) and (b) indicates a linear regression of *GPP* in urban sites from Awal et al. (2010), Crawford and Christen (2015), Velasco et al. (2016), and Menzer and McFadden (2017) and *NEE* from Hong et al. (2019b) and references therein scaled with vegetation fraction, respectively. See main texts for more information.

880



885

Figure 13. Monthly sums for gap-filled  $F_C$  (yellow bar) with  $RE$  (red bar),  $E_R$  (blue bar),  $E_B$  (gray bar), and  $-GPP$  (green bar)